World Electric Vehicle Journal

MDPI

Review

Review of State-of-Charge Estimation Methods for Electric Vehicle Applications

Miguel Antonio Pisani Orta [†], **David García Elvira** [†] **and Hugo Valderrama Blaví** [*,†]

Higher Technical School of Engineering, Universitat Rovira i Virgili, 43007 Tarragona, Spain; miguelantonio.pisani@urv.cat (M.A.P.O.); david.garciae@urv.cat (D.G.E.)

* Correspondence: hugo.valderrama@urv.cat; Tel.: +34-616-14-41-05

† These authors contributed equally to this work.

Abstract: Continuous and accurate state-of-charge estimation is essential for optimal reliability and performance in electric vehicle battery management systems. This work reviews state-of-charge estimation strategies, from straightforward methods like lookup tables and ampere-hour counting to advanced mathematical models, such as electrochemical, observer-assisted equivalent circuit, and impedance-based models that capture cell dynamics. Additionally, data-driven models including fuzzy logic, neural networks, and support vector machines are explored for their ability to leverage large datasets. This review highlights the strengths and limitations of each method, emphasizing the specific contexts in which these strategies can be applied to achieve optimal effectiveness.

Keywords: state-of-charge estimation; mathematical models; data-driven models; neural networks

Academic Editor: Grzegorz Sierpiński

Received: 9 January 2025
Revised: 31 January 2025
Accepted: 7 February 2025
Published: 9 February 2025

Citation: Pisani Orta, M.A.; García Elvira, D.; Valderrama Blaví, H. Review of State-of-Charge Estimation Methods for Electric Vehicle Applications. *World Electr. Veh. J.* **2025**, *16*, 87. https://doi.org/10.3390/wevj16020087

1. Introduction

Electric vehicles are widely recognized as a clean transportation alternative that lowers reliance on fossil fuels [1], contributing to efforts to combat environmental damage and the ongoing energy crisis [2]. The rapid advancement of electric vehicle technologies has driven research efforts towards developing accurate and reliable methods for estimating the state-of-charge (SOC) of lithium-ion cells [3]. A precise SOC estimation enhances safety and optimizes the use of stored energy. The primary motivation for optimizing energy usage in electric vehicle batteries lies in both practical and economic factors. Battery packs represent a significant cost component of electric vehicles, so maximizing their lifespan is essential. In addition, an accurate SOC estimation can reduce drivers' range anxiety, allowing them to plan when and where to recharge the batteries.

Electric vehicles' operation requires constant updates for the following: (1) the energy available in the battery pack (which directly correlates with the remaining driving range), and (2) the power capabilities (which determine the rate at which energy can be withdrawn from the battery without exceeding the safety limits set by the manufacturer) [4]. Thus, three key battery performance parameters emerge: SOC, state of health (SOH), and state of power (SOP). Energy and power cannot be measured directly due to the lack of a sensor capable of making such a measurement. For that reason, these quantities must be estimated using measurements of voltage $v(t)$, current $i(t)$, and temperature $T(t)$ [5] (see Figure 1).

The SOC represents the amount of ampere-hours that can be withdrawn from a cell (Q_{rem}) as a percentage of its maximum available capacity (Q_{max}): $\text{SOC} = (Q_{rem}/Q_{max}) \cdot 100\%$ [6]. Accurate estimates of the SOC not only provide real-time information on the energy available in the cell [7], but also offer benefits such as extending the cell's lifespan

by preventing harmful scenarios like overcharging and over-discharging, which lead to degradation and permanent damage to the battery [4,8].

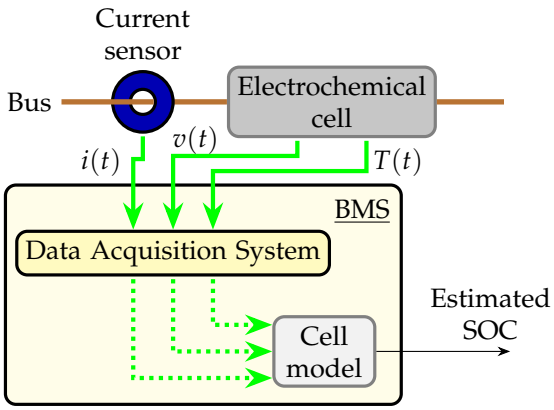

Figure 1. SOC estimation scheme in a battery management system (BMS).

The SOH indicates the battery's ability to store and deliver energy compared to when it was new. The SOH gradually declines over time due to aging factors, leading to a corresponding reduction in capacity. As mentioned before, the primary causes of capacity loss are internal aging mechanisms such as loss of lithium inventory, active material decomposition, and structural changes.

The SOP (in units of W) defines the maximum power a battery can consistently deliver or absorb within a predetermined time interval, without breaching design constraints [9]. The SOP ensures an optimal matching between the battery system and vehicle acceleration and climbing requirements, and also maximizes regenerative braking efficiency. The SOP decreases over time due to the increase in the cell's internal resistance. The resistance growth, on the other hand, is primarily attributed to the development of the solid electrolyte interphase (SEI) layer [10].

SOC, SOP, and SOH are closely interrelated, and accurate estimation of each state positively influences the others in a co-estimation framework. Specifically, precise SOC estimation plays a pivotal role in ensuring reliable SOP predictions in several ways, such as the following:

- An accurate SOC estimation enhances open-circuit voltage (OCV) predictions, which directly improves the accuracy of terminal voltage predictions under load conditions. This is particularly important for SOP estimation under voltage constraints [11];
- A reliable SOC estimation enables precise determination of the peak charge/discharge currents the battery can sustain without breaching safety limits, which is essential for accurate SOP estimation under current constraints [11].

Additionally, SOC estimation that incorporates the effects of battery aging and temperature variations can dynamically adjust SOP predictions to reflect the battery's current state. This ensures that SOP estimation remains accurate and reliable throughout the battery's lifecycle.

In electric vehicle applications, SOH is often estimated by analyzing the reduction in cell capacity through partial discharge cycles. This involves comparing the amount of charge extracted from the cell (ΔSOC) with the corresponding SOC variation (ΔSOC_{OCV}) derived from the OCV-SOC relationship. $SOH = (\Delta SOC / \Delta SOC_{OCV}) \cdot 100\%$ shows how an accurate SOC estimation from the outset is critical for this approach [12].

Another method for SOH estimation involves constructing an incremental capacity curve by monitoring capacity variations corresponding to fixed voltage changes [13]. The incremental capacity curve is characterized by several peaks, whose area, magnitude,

shape, and location represent different degradation mechanisms, such as the loss of lithium inventory, loss of active material, and the formation of lithium plating layers [13,14].

Among these performance parameters (SOC, SOH, and SOP), this document focuses on SOC, reviewing various estimation methods and analyzing the feasibility of applying them in electric vehicle applications. Section 2 provides an overview of some SOC estimation methods found in the literature. Section 3 summarizes the SOC estimation methods studied, highlighting their main strengths and weaknesses. And finally, Section 4 concludes by presenting the methodological limitations encountered in comparing the estimation methods, as well as future work and research guidelines.

2. State-of-Charge Estimation Methods

Over the years, various strategies have been developed to accurately estimate the SOC in electrochemical cells. These strategies can be broadly classified into four categories (see Figure 2): lookup table methods, direct-counting methods, mathematical model-based methods, and data-driven approaches [15].

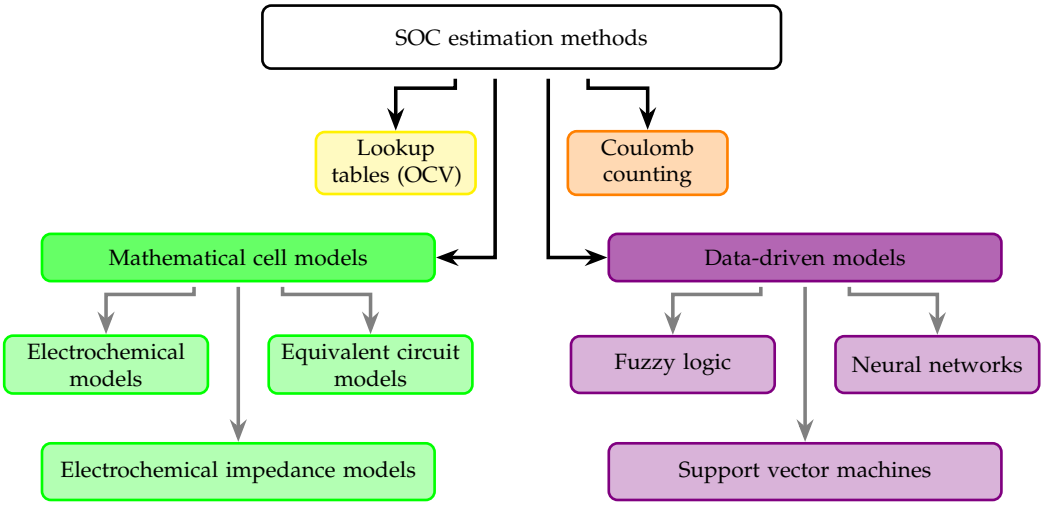

Figure 2. Classification of SOC estimation methods.

While simpler techniques like lookup tables and Coulomb counting remain useful, mathematical and data-driven models have been gaining high popularity in recent years [16,17]. Among these, electrochemical models (EM), equivalent circuit models (ECM) [18,19], and artificial neural networks (ANN) [20,21] are particularly prominent, each offering unique advantages in capturing the complex dynamics of SOC estimation. The following subsections present these estimation methods, examining their key advantages and limitations for application in the electric vehicle industry. After reviewing these SOC estimation methods, three use cases of ANNs combined with mathematical-based SOC estimation methods are analyzed in Section 2.4.4, highlighting the ability of data-driven methods to facilitate fusion or hybrid approaches.

2.1. Lookup Table Method

The lookup table method implements a direct relationship between the SOC and the OCV of an electrochemical cell. The OCV refers to the voltage measured between the positive and negative electrodes of a battery after it has been disconnected, allowing it to rest for a sufficient period of time, typically from one to three hours [21].

To generate such lookup tables, a very small current is applied to the battery cell while the accumulated ampere-hours and cell terminal voltages are logged [22]. Then, to estimate the SOC, the value stored in the lookup table corresponding to the current OCV is assigned.

This estimation method is very simple and easy to implement. However, it has limitations that make it unsuitable for electric vehicle applications. Two conditions must be met to obtain high accuracy when using the OCV method to estimate the SOC: (1) the electrochemical cell must initially be in an equilibrium state (quasi-thermodynamic stability) to minimize polarization voltage [23], typically achieved by allowing the cell to rest for two or more hours. Then, (2) the current applied or withdrawn from the battery should be zero. If not, it should be minimal (a rare condition in automotive settings) to reduce the voltage drop across the cell's internal resistance [24]. When these conditions are met, the cell terminal voltage will converge to the OCV.

The main drawback is that the OCV curve in the 20% to 80% SOC range is quite flat. This characteristic is especially evident in $LiFePO_4$ cells, but it is also noticeable in other lithium-ion chemistries. This flatness means that small variations in the measured terminal voltage, often due to sensor noise and sensor precision, can lead to significant errors in SOC estimation when using lookup tables. In other words, this method is highly sensitive to changes in OCV within this range. Furthermore, varying temperature conditions correspond to different SOC curves, although less significantly (see Figure 3a). To further enhance SOC estimation, lookup tables for various temperatures can be utilized, with interpolation performed for the specific temperature to determine the SOC.

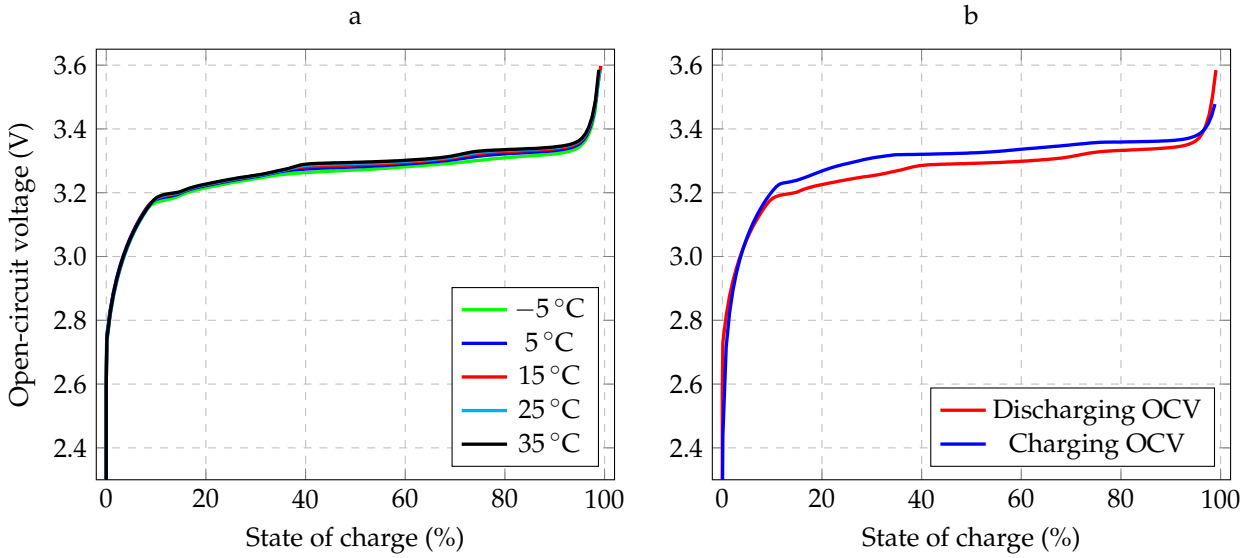

Figure 3. (**a**) Discharging OCV of a $LiFePO_4$ cell at different temperatures [4]. (**b**) OCV hysteresis phenomenon on a $LiFePO_4$ cell at 25 °C.

An additional challenge to estimate SOC is the OCV hysteresis (see Figure 3b). This phenomenon has been well documented in many battery types like nickel–metal hydride (NiMH) cells [25,26] and in lithium-ion chemistries like lithium iron phosphate ($LiFePO_4$), and lithium titanate ($Li_4Ti_5O_{12}$) [27]. The hysteresis effect describes a significant difference in the OCV at a given SOC after reaching equilibrium, depending on whether the battery was previously being charged or discharged. This effect is mostly generated by mechanical stress [28,29], thermodynamic effects in the electrode potentials [30], and the varying lithium insertion rates into the particles within an electrode [27]. The magnitude of hysteresis may depend on the type of chemistry employed. For example, for lithium-ion battery cathodes consisting of nanosized doped $LiFePO_4$, a value of approximately 7 mV of hysteresis was reported in [27]. According to [30], the hysteresis voltage can extend from a few millivolts in lithium cobalt oxide ($LiCoO_2$) to several tens of millivolts in lithium iron silicate (Li_2FeSiO_4) and titanium dioxide (TiO_2) cathodes. Consequently, a basic OCV-SOC

relationship without accounting for hysteresis effects can lead to larger SOC estimation errors [31].

Furthermore, the relationship between the SOC and OCV is not a simple one-to-one match; OCV is also influenced by charge–discharge rates [21,32], and to a lesser extent, temperature. Thus, relying solely on OCV for SOC estimation becomes even less reliable in practical applications, requiring the use of more sophisticated models, or using correction techniques to account for these influencing factors and improve accuracy.

2.2. Ampere-Hour Counting (Coulomb Counting)

Ampere-hour counting is one of the most used methods to estimate the SOC [33,34]. This method simply calculates the amount of charge entering and exiting the electrochemical cell over a certain period of time [35]. If known with some uncertainty (represented by the symbol "ˆ") the initial SOC ($\hat{z}_0$), the cell capacity ($\hat{Q}$), charge efficiency ($\hat{\eta}$), and the applied current to the cell (i_{meas}), the SOC can be computed as follows:

$$\hat{z}_k = \hat{z}_0 - \frac{\Delta t}{\hat{Q}} \sum_{j=0}^{k-1} \hat{\eta}_j \cdot i_{\text{meas},j} \tag{1}$$

where Δt denotes the sampling interval, the current $i_{\text{meas}} > 0$ for discharging processes, and $i_{\text{meas}} < 0$ for charging scenarios [4].

Analyzing this equation, if the initial SOC estimation ($\hat{z}_0$) is not completely correct, the final SOC estimation ($\hat{z}_k$) will preserve the initial error [36]. Other sources of error are determined by the estimates made on the cell capacity ($\hat{Q}$) and charge efficiency ($\hat{\eta}$). The charge efficiency or Coulombic efficiency is defined as the ratio of the discharge capacity to the charging capacity within the same cycle. Factors such as electrolyte decomposition, material aging, ambient temperature, and varying charge–discharge current rates influence the battery's charge efficiency. It typically remains below one, as some energy is consumed by the battery's internal resistance, resulting in the discharged electrical energy being less than the energy charged [37]. The lost charge is considered an indicator of parasitic reactions occurring within the cell, which contribute to capacity degradation or an increase in internal resistance [38].

Last but not least, the measured current (i_{meas}) includes random measurement noise and nonlinear errors associated with the measurement circuit. Additionally, the measured current (i_{meas}) neither reflects the current supplied by the cell to power the electronic circuit that monitors its performance, nor the self-discharge current of the cell [24].

The combination of all these sources of error will undoubtedly have a negative impact on the SOC estimate. As time passes, the error will accumulate and the reliability of the estimate will decrease [33,39]. Consequently, the SOC estimation technique using the Coulomb counting method is appropriate for short periods of operation where the initial conditions are well known [24]. Therefore, this technique is not fully recommended for applications where electric vehicles are exposed to long periods of use [40].

Nevertheless, the ampere-hour counting method can be improved by using the OCV curve to estimate SOC during rest or idle periods. As a result, the cumulative error from the Coulomb counting integration will be reduced. According to this, Ref. [40] carried out a study where the OCV was used to update the SOC estimate performed by the Coulomb counting when the cell was at rest for periods of one hour, obtaining absolute errors below 3% in the SOC estimation.

2.3. Mathematical Cell Models to Estimate the State-of-Charge

While the simpler SOC estimation strategies discussed earlier have limitations for real-time applications in electric vehicles, mathematical models offer a more sophisticated

approach. By incorporating various factors into mathematical equations, these models seek to capture the internal mechanisms of the cell, enabling recursive SOC estimation [15,41]. Developing such models requires a deep understanding of the electrical and chemical properties of the cell to achieve the desired robustness [42]. Mathematical cell models are typically classified into three main categories [7]:

- Electrochemical models;
- Equivalent circuit models;
- Electrochemical impedance models.

2.3.1. Electrochemical Models

The EMs are developed on the basis of complex nonlinear partial differential equations (PDEs) [43] and are derived from porous electrode and concentrated solution theories [44]. These models have the potential to accurately predict the behavior of a cell and provide detailed information about the internal states of the battery (lithium concentration, electrochemical and diffusion kinetic processes, potential gradients, etc. [45,46]) through the use of physical parameters that characterize the battery cell [4].

One of the most used EMs for estimating battery SOC is the one-dimensional (1D) model (see Figure 4). This model was proposed by Newman, Doyle, and Fuller in [47] and it describes the mass (movement of lithium ions) and energy (heat generation and dissipation due to resistive losses and electrochemical reactions) of each species for each domain (anode, cathode, separator) of a battery cell [7].

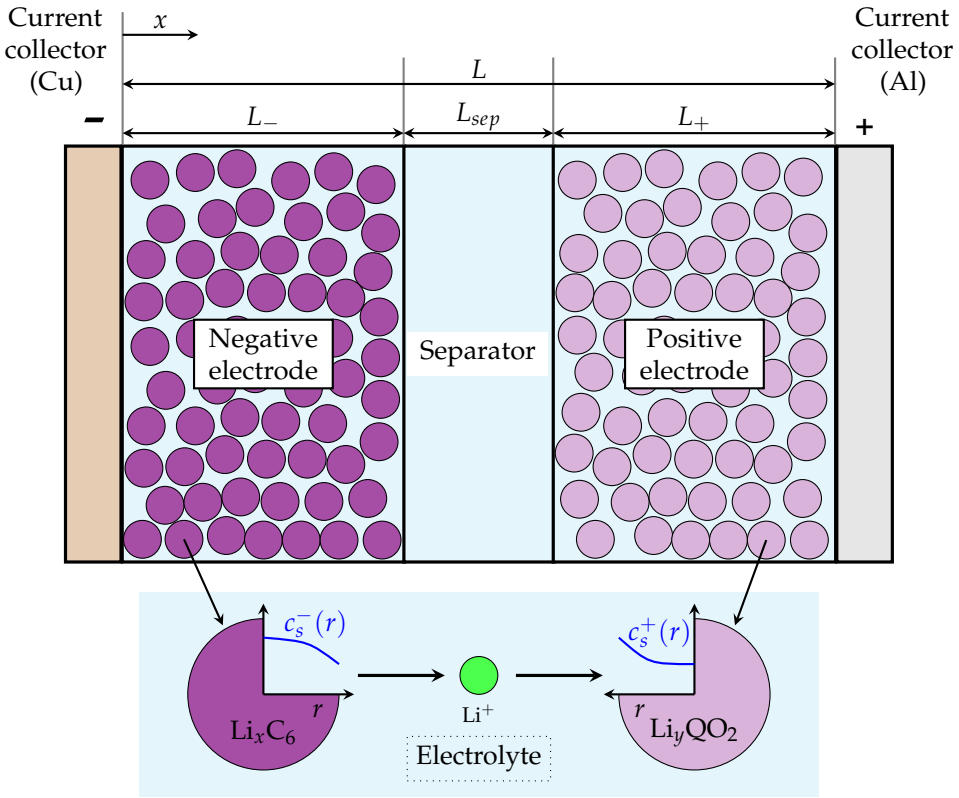

Figure 4. Schematic of 1D electrochemical model for lithium-ion cells [48].

The model is able to predict the discharge behavior of dual insertion cells and can be used to simulate any cell utilizing two composite electrodes composed of a mixture of active insertion material, electrolyte, and inert conducting material [49]. The inert conducting material in the composite electrodes is typically carbon black, chosen for its ability to provide an efficient pathway for electron transport within the electrodes, ensuring uniform

current distribution. Additionally, it remains chemically stable during battery operation as it does not participate directly in electrochemical reactions. A dual insertion cell (typically used in lithium-ion batteries) refers to a type of electrochemical cell in which both electrodes operate by insertion or intercalation of lithium ions into their material structures with little or no structural modification of the active materials during the charge–discharge reactions. Dual insertion cells are distinct from other battery chemistries such as nickel cadmium (NiCd) and NiMH where chemical reactions at the electrodes might involve more severe plating or deposition of materials [50].

The 1D electrochemical model involves three domains: the negative composite electrode (with Li_xC_6 active material), separator, and positive composite electrode (with Li_yQO_2 metal oxide active material). In the composite electrodes, the solid phase (typically modeled as spherical particles of uniform radii in the μm scale [51]) and the electrolyte phase are treated as superimposed continua [52]. This means the solid and electrolyte are modeled as if they are smoothly distributed through the same volume, ignoring the precise physical boundaries of the individual solid particles and electrolyte-filled pores [53]. In the model developed by Newman, Doyle, and Fuller, a solid polymer electrolyte was considered [47]; however, lithium perchlorate in a propylene carbonate liquid electrolyte has also been used as an alternative [49]. The transportation of lithium ions occurs from the negative electrode through the separator into the positive electrode during discharge via diffusion—and vice versa during charge.

The 1D electrochemical model consists of four PDEs describing the conservation of charge in the electrolyte phase (ϕ_e), the conservation of charge in the solid phase (ϕ_s), the concentration of lithium in the electrolyte phase (c_e), and the concentration of lithium in the solid phase (c_s) [43,54,55]. These equations are presented next:

$$\frac{\partial}{\partial x}\left(\kappa^{\text{eff}}\frac{\partial}{\partial x}\phi_e\right)+\frac{\partial}{\partial x}\left(\kappa_D^{\text{eff}}\frac{\partial \ln c_e}{\partial x}\right)+j^{\text{Li}}=0 \tag{2}$$

$$\frac{\partial}{\partial x}\left(\sigma^{\text{eff}}\frac{\partial}{\partial x}\phi_s\right)-j^{\text{Li}}=0 \tag{3}$$

$$\frac{\partial(\varepsilon_e c_e)}{\partial t}=\frac{\partial}{\partial x}\left(D_e^{\text{eff}}\frac{\partial}{\partial x}c_e\right)+\frac{1-t_+^0}{F}j^{\text{Li}} \tag{4}$$

$$\frac{\partial c_s}{\partial t}=\frac{D_s}{r^2}\frac{\partial}{\partial r}\left(r^2\frac{\partial c_s}{\partial r}\right) \tag{5}$$

As observed in the previous set of equations, electrochemical models require a large number of parameters. These parameters can be classified as either transport, thermodynamic, or design-adjustable parameters [56], and they can be obtained by experimentally characterizing the inherent properties of the materials being used to fabricate the cell. The transport properties of the solution/electrolyte phase include the following:

- The effective ionic conductivity of an electrolyte (κ^{eff}) refers to its ability to conduct ions under an electric field, accounting for the properties of both the electrolyte itself and its interaction with the surrounding environment. It is typically in units of S/cm [56];
- The effective ionic diffusional conductivity of an electrolyte (κ_D^{eff}) accounts for how the movement of cations and anions, influenced by concentration gradients, contributes to the overall ionic conductivity. It is expressed in units of S/cm [56];
- The effective diffusion coefficient of lithium salt in the electrolyte (D_e^{eff}) describes how lithium ions diffuse through the electrolyte, considering the effects of the medium's porosity and tortuosity. The effective diffusion coefficient has units of cm^2/s [56];

- And the transference number of lithium ion with respect to the velocity of solvent (t_+^0) is defined as the ratio of the electric current derived from the cation to the total electric current [57]. This parameter is dimensionless.

The transport properties of the solid phase include the following: the effective electronic conductivity of the electrode solid matrix (σ^{eff}), expressed in S/cm, and the diffusion coefficient of lithium in the solid electrode particles (D_s), expressed in cm^2/s.

Thermodynamic properties for the overall cell reaction are mainly included in j^{Li}, characterizing the flux of lithium ions in the electrodes. The design adjustable properties comprise the average particle radii (r) for the insertion material particles, component thicknesses, initial SOC in the electrodes, initial cell temperature, etc. [56]. The volume fraction and the Faraday constant are represented by ε_e and F, respectively.

The parameters obtained for an electrochemical model of a battery are typically chemistry-specific and can be useful for modeling other batteries with the same chemistry. However, cell-specific factors such as electrode design, manufacturing variations, and aging can cause alterations in parameters. Therefore, the uncertainty in electrochemical parameters can limit the accuracy of EMs, creating a biased estimate of the internal states of the cell [46]. Additionally, extracting the parameters for these models typically requires destructive testing, which can be both time-consuming and costly. Such tests are performed to thoroughly characterize the battery's internal composition and reactions, but this also restricts the practicality of EMs, especially for on-the-go applications where non-destructive estimation is needed.

Despite these challenges, various implementations of electrochemical models for estimating SOC have been explored in the literature. A Kalman filter-based observer was implemented on a reduced-order single-particle EM for estimating both the solid-phase surface lithium concentration and the battery SOC [58]. The lithium concentration in the cathode was estimated with an error of less than 1%, while the SOC, which correlates with changes in the average lithium concentration in the negative electrode, was estimated with an error below 0.5%.

Similarly, a reduced-order electrochemical model using a Luenberger observer was proposed in [59]. In these simulations, the initial SOC was deliberately set to 60% of the actual value to evaluate the observer's robustness to initial condition inaccuracies. The simulations were conducted at discharge rates of $0.2C$, $1C$, $3C$, and $5C$, achieving mean SOC estimation errors of 0.32%, 1.66%, 5.01%, and 9.86%, respectively, showing that at high discharge rates, this model lacks precision.

Last but not least, the main drawback of EMs is that solving the PDEs is computationally demanding, requiring substantial resources like processing power, memory, and time due to the complexity and nature of these equations. This high computational cost limits the feasibility of using EMs in real-time applications [46]. Moreover, these PDEs are solved numerically rather than analytically, which can introduce additional accuracy issues.

To overcome the complexity of physics-based EMs and the computational burden of solving their PDEs, electrical ECMs and equivalent circuit impedance models have gained recognition due to their lower complexity. Among these, electrical ECMs, or integral-order models, offer the lowest accuracy and are discussed in Section 2.3.2. On the other hand, equivalent circuit impedance models, or fractional-order impedance models, provide higher accuracy but at the cost of increased complexity. These fractional-order models (FOMs) are presented in Section 2.3.3.

2.3.2. Observer-Assisted Equivalent Circuit Models

Equivalent circuit models use electronic components (resistors, capacitors, and voltage sources) to build a circuit network capable of describing the terminal voltage of the battery

taking into account the current profile applied to the cell to parameterize the model [4,7]. The equations describing the circuit detail with precision various dynamic behaviors of the battery. The simplicity and robustness offered by ECMs constitute the main reasons for being widely used in a BMS to estimate the SOC. One of the most used ECMs is the enhanced self-correcting (ESC) cell model [4] illustrated in Figure 5. The OCV as a function of the SOC is represented by a voltage-dependent source. The cell current is represented with the notation $i(t)$; $i(t) > 0$ in discharge processes, and on the contrary, $i(t) < 0$ when the cell is being charged; $v(t)$ is the cell terminal voltage and i_{R_1} represents the diffusion current flowing through the resistor R_1. The series resistance R_0 describes the internal resistance of the electrochemical cell. Lithium diffusion processes in lithium-ion cells result in a voltage that changes slowly when current is applied or demanded from the cell. To approximate this behavior, a parallel network R_1C_1 is included in the model, where the diffusion voltage will be represented by the voltage associated with the resistor R_1 [54]. Finally, a block called "Hysteresis" describes the hysteresis $h(t)$ in the terminal voltage commonly observed in lithium-ion and NiMH cells.

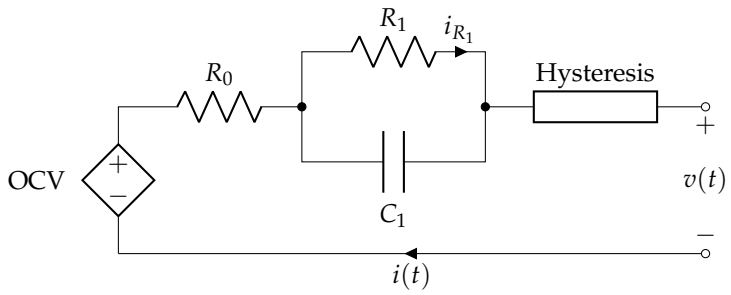

Figure 5. Enhanced self-correcting cell model [4].

ECMs incorporate Coulomb counting within their equations to estimate the SOC. By tracking the current flowing into and out of the battery, Coulomb counting provides a direct calculation of charge levels. However, to enhance accuracy, the estimation process leverages observer filters, such as Kalman filters, that use the measured terminal voltage as feedback. This feedback mechanism continuously corrects the SOC estimate, even if the initial estimate deviates from the actual value. As a result, the model progressively refines the SOC estimate over time, compensating for potential errors and providing a highly accurate final result.

For simplicity in notation, the SOC is represented as $\mathrm{z}(t)$. The ordinary differential equations (ODEs) that describe the dynamic aspects of the ESC cell model [$\mathrm{z}(t)$, $i_{R_1}(t)$, $h(t)$] are presented as follows:

$$\dot{\mathrm{z}}(t) = \frac{-\eta(t)i(t)}{Q} \tag{6}$$

$$\dot{i_{R_1}}(t) = -\frac{1}{R_1C_1}i_{R_1}(t) + \frac{1}{R_1C_1}i(t) \tag{7}$$

$$\dot{h}(t) = -\left|\frac{\eta(t)i(t)\gamma}{Q}\right|h(t) + \left|\frac{\eta(t)i(t)\gamma}{Q}\right|M(\mathrm{z},\dot{\mathrm{z}}) \tag{8}$$

where γ is used as a positive constant to fit the equation and the term $M(\mathrm{z},\dot{\mathrm{z}})$ is a function that explains the maximum polarization due to hysteresis as function of SOC and its rate of change [4]. The equation describing the cell terminal voltage is the following [4]:

$$v(t) = \mathrm{OCV}(\mathrm{z}(t)) + h(t) - R_1 i_{R_1}(t) - R_0 i(t) \tag{9}$$

Subsequently, it is very common to use this set of equations in their state-space form and apply different observers (extended Kalman filter (EKF), unscented Kalman filter (UKF), particle filter, Luenberger observer, H_∞ observer, etc.) to estimate the internal states of the model, including the SOC. In [24], an estimate of the SOC was obtained using the EKF with an mean-squared error (MSE) less than 3%. In [60], the accuracy of the SOC estimation via EKF and UKF observers was compared utilizing the Thevenin equivalent circuit model (identical to the ESC cell model without the hysteresis block [61]), obtaining errors less than 2.5%. In [62], a UKF and a particle filter were proposed to improve the adaptability to non-Gaussian noise. They used a second-order *RC* model (Thevenin model with two *RC* parallel networks) and obtained a root-mean-squared (RMS) error of 0.61%.

Summarizing, ECMs include a series of ODEs that can be easily implemented in BMS microcontrollers. Thus, algorithms running on these types of models do not require as much processing power as those of EMs. On the other hand, when using ECMs to estimate SOC, we must take into account errors associated with the estimated cell capacity (Q), errors due to modeling, and errors derived from current and voltage sensors. And last but not least, the resulting model should not be applied in scenarios very different from those from which the data were originally collected to parameterize the model [4].

To address the limitations of ECMs, which stem from their reliance on fixed model parameters, the implementation of an algorithm capable of real-time parameter estimation would be highly beneficial. In this context, Ref. [63] proposed a recursive method for online parameter identification integrated with SOC estimation. This approach, applied to a Thevenin equivalent circuit, was evaluated using a hybrid driving profile combining the Urban Dynamometer Driving Schedule (UDDS) and Federal Urban Driving Schedule (FUDS) cycles. The robustness of the method was validated by introducing white Gaussian noise with standard deviations of 2 mA and 2 mV to simulate low data quality. Its convergence capabilities were also tested by offsetting the initial values of the model parameters, with results indicating that the method converged quickly, demonstrating promising traceability. Additionally, its performance was benchmarked against three variants of the forgetting factor recursive least squares method, chosen for their well-known traceability and computational efficiency [63]. Numerical results highlighted that the proposed method achieved the lowest mean-squared deviation in model parameter error, at -20.17 dB, outperforming all the compared methods. This indicates that adopting online (real-time) parameter estimation could serve as a promising solution to mitigate the inherent drawbacks of ECMs.

2.3.3. Electrochemical Impedance Models

Electrochemical impedance models can be categorized into two subgroups: models based on the electrochemical impedance spectroscopy (EIS) method, which characterize the cell in the frequency domain, and FOMs, which leverage fractional calculus to capture the batteries' more complex properties. This subsection provides a review of both subgroups, examining their underlying principles, advantages, and limitations.

The technique based on EIS determines a set of SOC-dependent parameters that characterize the cell in a wide range of frequencies. This method applies to the battery a small-amplitude sinusoidal voltage (usually between 5 mV and 50 mV) in a frequency range between 0.001 Hz and 100 kHz [64]; by means of measuring the current amplitude and phase shift at each frequency, the resistive and reactive components of the impedance are determined. For all this, the impedance spectroscopy technique represents a very useful tool to describe the dynamic behavior of electrochemical cells at any point of operation [7].

In [65], a kernel density estimation method (using a normal-type kernel) was proposed to investigate correlations between the SOC and impedance measurements of $LiFePO_4$ batteries during discharge cycles. Kernel density estimation is a statistical technique where

the data samples solely determine the probability density function (PDF) of a random variable [66]. For each SOC level, a PDF was estimated for the real part and another PDF for the imaginary part of the impedance. The resulting probability density functions (characterized by peak and width values) revealed that, for the real component of the impedance, the peak value increases as the SOC increases almost linearly, showing a potential positive correlation with the SOC. On the other hand, the width value of the PDF decreases as the SOC increases almost linearly, showing a potential negative correlation with the SOC.

In [67], the enhancement of SOC estimation was explored by using support vector machines (SVM), incorporating impedance information alongside conventional inputs of voltage, current, and temperature. An in situ electrochemical impedance spectroscopy technique was carried out by superimposing a multi-sine current signal (in the frequency range 10 mHz to 100 Hz) on a DC component generated by a boost converter. Constant-current discharge profiles applied to 3.2 Ah $LiFePO_4$ cells achieved RMS error values of 1.06% and 1.09% for SOC estimation with impedance data at 100 mHz and 100 Hz, respectively.

The electrochemical impedance models (EIM), originally developed to match impedance spectra in the frequency domain, have been adapted for use in the time domain for purposes such as voltage simulation and SOC estimation. These adaptations have led to the emergence of FOMs [68] or equivalent circuit impedance models.

Equivalent circuit impedance models have also emerged with the goal of providing physics-based parameters while minimizing approximation errors, such as those related to electrical voltage response. These models are particularly useful for simplifying complex EMs through order reduction, as the latter often require numerical solutions that can take several minutes to hours to obtain (posing significant challenges for implementation in on-board BMSs). Additionally, the physics-based parameterization of equivalent circuit impedance models (see Figure 6) enables the extrapolation of battery behavior to unmeasured operating conditions, as parameter variations adhere to physical constraints [69]. This makes these models especially suitable for applications where interpreting the physical significance of parameter changes is a key objective [69].

The FOMs, unlike the ECMs analyzed in Section 2.3.2, include other parameters besides resistors, capacitors, and voltage sources—for example, constant phase elements (CPEs) and the Warburg impedance [7,42,54]. The CPEs describe the non-ideal capacitance due to the non-uniform distribution of materials and textures at interfaces. CPEs are fractional-order elements [68] whose impedance at frequency f is expressed as follows:

$$Z_{\mathrm{CPE}}(\omega) = \frac{1}{Q(j2\pi f)^{\alpha}} \tag{10}$$

where $Q(s^{\alpha}/\Omega)$ and α give the coefficient and order, respectively. CPEs are generalized elements that can represent the ideal capacitance ($\alpha = 1$) and resistance ($\alpha = 0$) [68].

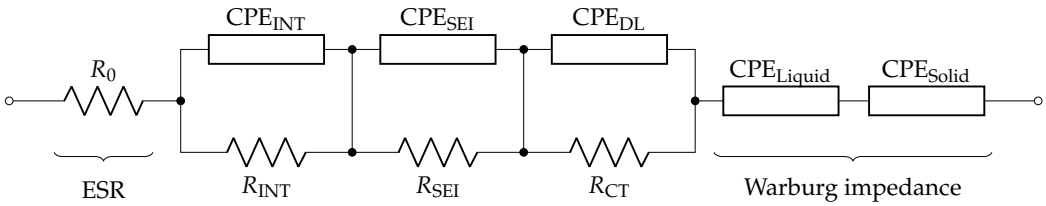

Figure 6. General equivalent circuit of impedance models [70].

Figure 6 illustrates an example of an $R_0(R||\mathrm{CPE})(R||\mathrm{CPE})(R||\mathrm{CPE})W$ equivalent circuit of an impedance model, consisting of a resistance R_0, three parallel $R||$CPE branches,

and a Warburg element arranged in series. The intrinsic meaning of each electrical component is described below:

- R_0 represents the equivalent series resistance (ESR), which includes all overpotentials that occur instantaneously after changing the current [69]. In other words, it quantifies the resistance of the electrolyte and the electrical conductivity of the electrodes and the connected wires [70];
- CPE_{INT} and R_{INT} represent the impedance caused by non-ideal contact within the interior of the electrodes [70]. This includes irregularities and imperfections in the electrode material that affect the overall charge transfer and storage behavior in the battery;
- CPE_{SEI} and R_{SEI} symbolize the layers of the SEI at the interfaces between the electrolyte and the electrodes [70]. These components account for the resistive and capacitive effects of the SEI, which influence ion transport and charge transfer during battery operation;
- R_{CT} represents charge transfer resistance, which corresponds to the overpotentials generated by charge-transfer reactions that occur when current is applied to a lithium-ion battery [70,71]. CPE_{DL} models the double-layer capacitance, capturing the effect of ions in the electrolyte aligning at the electrode–electrolyte interfaces due to the potential difference across the electrolyte. This alignment creates a capacitive behavior characteristic of the double-layer region [69];
- Finally, $\text{CPE}_{\text{Liquid}}$ and $\text{CPE}_{\text{Solid}}$ embody the Warburg impedance, which models the lithium ions' diffusion processes that are dominant at low frequencies [69].

FOMs are based on the Grünwald–Letnikov derivative D^{α} of a function $f(t)$, which enables the calculation of derivatives of non-integer order [68]. This derivative can be expressed as follows:

$$\text{D}^{\alpha} f(t) = \lim_{h \to 0} \frac{1}{h^{\alpha}} \sum_{i=0}^{\infty} (-1)^i \binom{\alpha}{i} f(t - ih) \tag{11}$$

where h denotes the sampling interval and $\binom{\alpha}{i}$ represents the Newton binomial coefficient [68]. This equation results in a memory effect that accounts for all values of $f(t)$ within the range $[0, t]$. To minimize computational expense, a short-memory principle is employed [68], limiting the data to the range $[t - L, t]$. This leads to the following modification:

$$\text{D}^{\alpha} f(t) \approx \frac{1}{h^{\alpha}} \sum_{i=0}^{L} (-1)^i \binom{\alpha}{i} f(t - ih) \tag{12}$$

where L denotes the memory length [68]. It is quite common to represent a fractional-order system using state-space equations for SOC estimation through observers such as Kalman filters. The following two equations provide a concise representation of a fractional-order system in state-space form:

$$\text{D}^{\alpha} \boldsymbol{x}_{k+1} = \boldsymbol{f}(\boldsymbol{x}_k, u_k) + \boldsymbol{w}_k \tag{13}$$

$$y_k = g(\boldsymbol{x}_k) + v_k \tag{14}$$

where $\boldsymbol{x}$ is the state vector, y is the measurement, u is the input, and w and v represent the process noise and measurement noise, respectively [68]. The mathematical formulations detailing the discretized state-space representation for SOC estimation across five different FOMs are thoroughly presented in reference [68]. The five FOMs compared in [68] have the following structure: (1) $R_0(R||\text{CPE})$; (2) $R_0(R||\text{CPE})W$; (3) $R_0(RW||\text{CPE})$; (4) $R_0(R||\text{CPE})(R||\text{CPE})$; and (5) $R_0(R||\text{CPE})(R||\text{CPE})W$.

A fractional-order multi-model system was developed in [72] by integrating three sub-models, allowing for adaptability across various temperatures and dynamic driving profiles. Each sub-model utilized the $R_0(R||\text{CPE})$ configuration. The Dynamic Stress Test (DST) was performed at three distinct temperatures (−5 °C, 20 °C, and 45 °C) to parameterize the sub-models, which resulted in maximum voltage errors of 50 mV during the fitting process. Experimental data were collected at a rate of 1 Hz throughout all battery tests. To validate the SOC estimation, the UDDS and FUDS tests were conducted at temperatures of −5 °C, 5 °C, 20 °C, and 35 °C using the proposed UKF-assisted FOMs. The numerical results demonstrated the following: (1) an SOC mean-absolute error (MAE) below 1.220%; (2) RMS errors below 2.626%; and (3) rapid convergence even after imposing a 20% initial SOC error, showcasing the robustness and effectiveness of the model.

Similarly, in [73], a partial-adaptive fractional-order model with an $R_0(R||\text{CPE})(R||\text{CPE})$ structure was implemented. The novelty of this work lies in the partial-adaptive approach, which retains the parameters of the first $R||$CPE branch obtained offline while dynamically adjusting R_0 and the second $R||$CPE network. This method captures both slow and fast dynamics, ensuring accurate SOC estimation. For validation, under the UDDS profile, the partial-adaptive model achieved an SOC MAE of 0.601% and an RMS error of 0.652%; under the FUDS profile, it achieved an MAE of 0.359% and an RMS error of 0.477%.

Regarding computational efficiency, in both [72,73], all simulations were conducted in MATLAB, with average execution times of less than 1 ms. Even in worst-case scenarios where these algorithms are implemented on slower microcontrollers, these results demonstrate significant potential for integration into on-board BMSs, where the typical sampling period is 1 second.

In [68], a comprehensive comparison was conducted among five state-of-the-art UKF-aided FOMs for SOC estimation, leading to the following conclusions:

1. Increasing the complexity of FOMs does not always enhance the accuracy of terminal voltage modeling;
2. The evaluation of the five FOMs (compared under the DST and UDDS profiles at 25 °C) revealed that the simplest model structure, $R_0(R||\text{CPE})$, outperformed the others in SOC estimation accuracy, achieving an overall RMS error of 0.57%;
3. The impact of memory length (a key characteristic of FOMs) on SOC estimation was analyzed, revealing that SOC estimation error decreases as the memory length L increases. However, this comes at the cost of an increase of the overall computational time;
4. The filters designed at 25 °C were tested under temperature conditions of 15 °C and 35 °C, showing that more complex FOMs demonstrate greater robustness to temperature variations compared to the simpler $R_0(R||\text{CPE})$ structure;
5. The parameterized FOMs were utilized to estimate SOC across six different cells, exhibiting strong generalization capabilities with RMS errors below 2.5%. Among them, the simplest $R_0(R||\text{CPE})$ model achieved the highest estimation accuracy, with RMS errors under 0.6% and the lowest standard deviation in RMS SOC estimation error, recorded at 0.0259%;
6. The impact of voltage and current sensor drift was also examined, with voltage drift set to [−10,10] mV and current drift to [−200,200] mA. In both scenarios, the simplest $R_0(R||\text{CPE})$ model once again demonstrated superior precision.

Summarizing, electrochemical impedance spectroscopy has traditionally been limited to offline SOC estimation. However, recent advancements have demonstrated the feasibility of online evaluation by leveraging various perturbation sources, enabling impedance measurements without interrupting normal electric vehicle operation [74,75]. Despite these advancements, the high cost of equipment needed for spectroscopy is a primary limitation to the widespread adoption of this technique for SOC estimation in electric

vehicle applications. Additionally, the low impedance of electrochemical cells makes obtaining accurate impedance measurements challenging, as it requires detecting small voltage fluctuations in response to minimal current stimuli [71,76], often in highly noisy environments. As a result, impedance spectroscopy remains more suited to experimental or laboratory settings rather than real-time applications.

The transition of impedance models from the frequency domain to the time domain through fractional calculus marks a significant advancement in SOC estimation. With the inclusion of CPEs, FOMs more effectively capture the intricate electrochemical dynamics of batteries, improving both voltage modeling and SOC estimation, two critical components of modern BMSs. Moreover, FOMs exhibit acceptable compatibility with observers, as demonstrated extensively in [68,72,73]. This compatibility enables the integration of FOMs with filtering techniques, such as Kalman filters, even on low-cost microcontrollers. FOMs also show excellent generalization in SOC estimation across different cells [68], a highly desirable attribute for reducing computational overhead while maintaining performance. This is particularly valuable for electric vehicle battery systems, which consist of thousands of cells, where modeling each cell individually can be computationally intensive. However, the inherent memory effect of FOMs presents challenges. Reducing the memory length diminishes SOC accuracy, while increasing it raises computational costs. Additionally, the truncation error introduced by the short-memory principle depends on the models' structure and driving profiles [68]. This error violates the Kalman filter assumption that errors are white noise, potentially impacting the ability of FOMs to refine SOC estimation results.

2.4. Data-Driven Models to Estimate the State-of-Charge

Data-driven strategies basically use a collection of historical data from the system under study to develop a black-box model, which employs a nonlinear relationship between the input and the output to be estimated. Thus, the model can make decisions based on the outcomes from the training phase [7,77].

These models have several advantages, such as parallel processing, high computation rates, etc. Three of the most used algorithms in electric vehicle applications to estimate the SOC are reviewed below:

- Fuzzy logic method;
- Artificial neural networks;
- Support vector machines.

Section 2.4.4 also analyzes three fusion methods, emphasizing the applicability of ANNs in the development of hybrid approaches for SOC estimation.

2.4.1. Fuzzy Logic Method

Fuzzy logic is a computational approach that offers flexibility and facilitates the concept of partial truth or logic with multiple values. The actual value can vary from completely true, partially true, or completely false, depending on the degree of fulfillment of a premise [42]. In the fuzzification stage (see Figure 7), a raw quantity is converted into a fuzzy quantity [78], recognizing that many values considered exact inherently possess uncertainty.

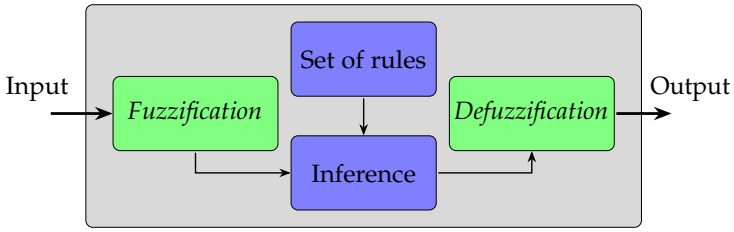

Figure 7. Basic structure of fuzzy logic system.

In real-world applications, measurements such as cell terminal voltage, current, and temperature are recorded by sensors and are thus prone to experimental errors. To implement fuzzy logic systems effectively, these scalar quantities must first be converted into membership functions (μ) (see Figure 8), allowing them to form the structured inputs required by the system.

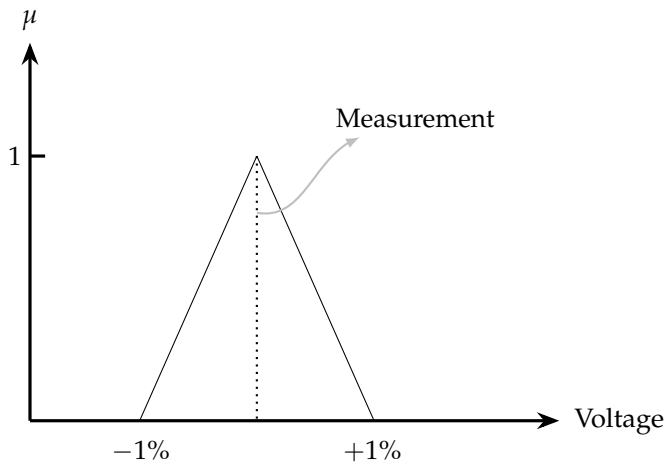

Figure 8. Triangular membership function of voltage sensor with accuracy of ±1%.

Next, fuzzy logic systems operate on a set of rules that express the relationship between input and output variables. This rule set, typically expressed as if–then statements, captures system knowledge and human reasoning in a natural, intuitive manner. The inference process then combines these rules to generate a fuzzified output. Through operations such as AND, OR, and NOT, based on fuzzy logic theory, information is linked across rules and input variables. The final output is a fuzzified response that represents the system's reaction to the given input conditions.

The final stage in these systems is defuzzification, where a fuzzy set with its corresponding degrees of membership is converted into a quantifiable value. This step is crucial when the system needs to deliver a quantitative result.

After explaining the main principles of fuzzy logic, the following paragraphs review its application in various studies. In [79], electrochemical impedance spectroscopy was conducted on NiMH cells at various SOC levels. Impedance measurements were taken at frequencies of 10 Hz, 251.1 Hz, and 3981.1 Hz. A five-input, Sugeno-based fuzzy logic model was then developed using the real and imaginary components of the impedance at 10 and 251.1 Hz, along with the real component at 3981.1 Hz, to predict the SOC with an error margin of ±5%. It was observed that at these three frequencies, variations in the real and/or imaginary components of the impedance offered sufficient distinction between successive SOC levels, thus justifying their selection.

An adaptive neuro-fuzzy inference system (ANFIS) was proposed in [80] to model electric vehicle batteries. The model used battery terminal voltage, discharge current, discharged capacity, and surface temperature as inputs. A 12 V, 40 Ah lead-acid battery was tested across five different operating profiles during experimentation. An average error of 0.53% was achieved with the training data, while validation on new driving profiles, distinct from those in the training phase, resulted in an approximate error of 2%.

A fuzzy logic approach combined with the Coulomb counting method was utilized in [81] to estimate the SOC of a lithium-ion battery. MATLAB Simulink was used to simulate the charging and discharging cycles of a 12 V, 100 Ah cell. The SOC estimation error was approximately 2% during charging and around 0.5% during discharging.

A hybrid model was proposed in [82] combining an extended Kalman–Bucy filter with a fuzzy logic controller. The topology was implemented in MATLAB Simscape and applied to a second-order *RC* model of the 4.2 V, 2.84 Ah Panasonic NCR18650PF lithium-ion battery. The SOC estimation achieved an MAE of 0.49% and an RMS error of 0.72%.

A fuzzy logic system was employed in [83] to design an SOC monitoring system for lead-acid batteries. Real-time SOC estimation was conducted during battery charging and discharging, using current, voltage, and temperature measurements as inputs. The fuzzy logic-based SOC estimations were compared to those obtained using the Coulomb counting method, with maximum errors reaching up to 10%.

In summary, fuzzy logic methods are highly effective at handling uncertainty, making them well suited for SOC estimation in conditions where sensor data may be noisy or imprecise. Their flexibility allows them to integrate expert knowledge and human reasoning directly into the estimation process, which is particularly valuable in complex or dynamic environments. However, despite these strengths, fuzzy logic techniques may struggle to achieve the high precision needed in applications where detailed and highly accurate modeling is essential. This limitation arises because fuzzy systems depend on the quality of the rule set and the membership functions defined, both of which can be difficult to refine to the necessary level of accuracy without extensive empirical tuning.

2.4.2. Artificial Neural Networks

Artificial neural networks are very popular techniques within the field of Machine Learning that simulate the learning process of biological organisms. Figure 9 illustrates an artificial neuron. The synapses are represented by weights $\boldsymbol{w}$, and the invariant terms of the prediction are represented by biases $\boldsymbol{\theta}$. Inside the artificial neuron, two processes are executed: (1) the addition of all scaled inputs, and (2) the application of an activation function ϕ to the value obtained in the summation.

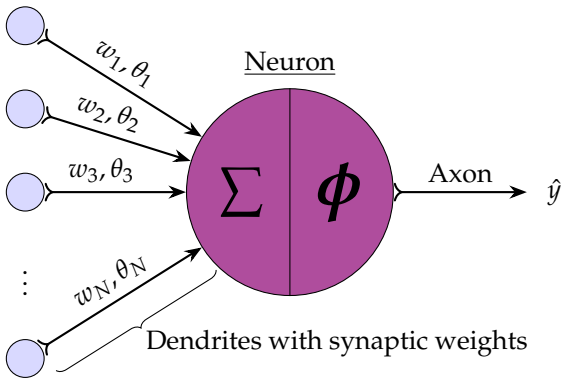

Figure 9. Basic structure of an artificial neuron.

Various nonlinear activation functions can be applied across different layers of ANNs to enhance their modeling capacity [84]. Common activation functions include the sign function, sigmoid, hyperbolic tangent, rectified linear unit (ReLU), softmax, among others. The estimated output value ($\hat{y}$) of an artificial neuron is then calculated using the following equation:

$$\hat{y} = \phi\left(\sum_{i=1}^{N} x_i w_i + \theta\right) \tag{15}$$

where the set $\{x_i; i = 1, \ldots, N\}$ represents the values at the input of the neuron prior to being modified by the weights in the corresponding synapses [84].

The basic structure of an ANN (see Figure 10) consists of an input layer that simply transmits the input information to the network. In the context of SOC estimation, the

input layer can receive measured variables such as terminal voltage, cell current, and cell temperature. Additionally, features such as the average of the previous M voltage and current measurements or past SOC estimations can be incorporated to help the network identify patterns between these inputs and the actual SOC. The intermediate (or hidden) layers use the backpropagation gradient-based training method to capture relevant features of the input at different levels of abstraction, enhancing the model's ability to generalize to unseen data during the training phase. Finally, the output layer computes the variable to be estimated, in this case, the SOC. However, an ANN can also be trained to output additional variables, such as SOH and terminal voltage.

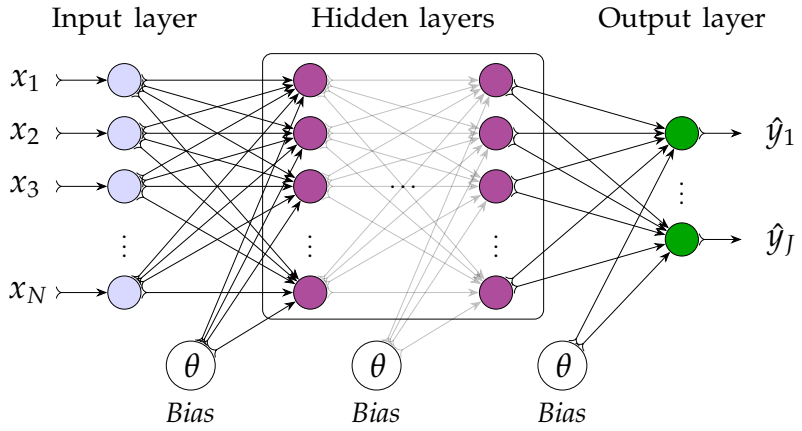

Figure 10. Architecture of an artificial neural network with multiple hidden layers.

There are several types of ANNs, each suited to specific tasks based on their distinct architectures and characteristics. The most common types are feedforward neural networks (FNN), convolutional neural networks (CNN), and recurrent neural networks (RNN). FNNs are the simplest type, where information flows in one direction from input to output [85]. These networks are typically used for general classification and regression tasks. CNNs are designed to process data with grid-like topology by using convolutional layers to detect spatial hierarchies in data. RNNs are specialized for sequential data, maintaining information from previous inputs, making them ideal for time series prediction tasks [86]. Variants of RNNs include long short-term memory (LSTM) and gated recurrent unit (GRU) networks for better handling long-term dependencies [86,87].

Brief summaries of reviewed articles that utilized various neural network architectures for state-of-charge estimation are presented next. In [88], four ANNs (FNN and RNN architectures) were implemented to estimate the SOC of a 4.2 V, 2 Ah rechargeable lithium polymer battery during charge (constant current–constant voltage) and discharge (constant current discharge at $C/2$) cycles. The FNN integrated two hidden layers: during charging it used 9 and 10 neurons for the first and second layers, respectively, and 10 and 8 neurons during discharging. The architecture of the RNN included two delays and 1 neuron in the hidden layer for charging, and one delay and 10 neurons in the hidden layer for discharging. Both networks had six inputs: battery voltage, current, battery temperatures at the anode, cathode, and surface, and ambient temperature. Results showed that the RNN achieved better SOC prediction accuracy during charging, with a relative error under 5%, while both ANNs maintained relative errors under 10% during discharge, with some underperformance noted.

A genetic algorithm was employed in [89] to optimize an FNN with three hidden layers, each containing 20 neurons. The network's inputs included voltage, current, temperature, and the average voltage and current calculated over the previous 500 one-second intervals to capture the battery's recent behavior. On the training set, an average error of

0.9% was achieved, with a maximum error of 1.3%. For the validation set, the average error was 2%, while the maximum error reached 13%.

The performance of a bidirectional LSTM network was compared with that of a traditional LSTM configuration in [90]. The experimental dataset consisted of profiles from four 4.5 Ah Tesla Model 3 cells tested under various drive cycles, including UDDS, Supplemental Federal Test Procedures (SFTP), Highway Fuel Economy Test (HWFET), and custom cycles with randomized segments of the standard cycles. The bidirectional LSTM network was structured with two hidden layers containing 10 nodes each, while the LSTM network had four hidden layers, also with 10 nodes per layer. Both models were trained using the ADAM optimizer. Results showed that the bidirectional LSTM network achieved RMS errors below 4.67%, while the traditional LSTM network achieved RMS errors below 4.54%.

A method was proposed in [91] to estimate the SOC of a 4.2 V, 2.9 Ah Panasonic 18650PF lithium-ion battery using a bidirectional GRU neural network optimized by a pigeon-inspired genetic algorithm. The feasibility of this method was tested across various temperatures under dynamic driving cycles, including Unified Cycle Driving Schedule (UCDS), SFTP, UDDS, DST, and FUDS. The proposed approach achieved an RMS error of 0.83%, outperforming other RNN architectures such as LSTM and GRU in terms of estimation accuracy.

Although ANNs can achieve strong performance, significant challenges arise during their training phase: (1) avoiding overfitting, which requires large datasets for effective training; (2) overcoming severe nonlinearities in the optimization function, which presents many local minima and requires adjustments to prevent the algorithm from getting stuck or facing convergence issues; and (3) the high computational demand due to the extensive calculations needed to update parameters across multiple layers, especially as training datasets grow.

It is evident that ANNs differ from mathematical-based cell models in terms of functionality (see Table 1). The latter rely on deterministic formulas or equations derived from physical principles or circuit behavior. In contrast, ANNs require training on historical data to learn patterns and relationships rather than directly applying predefined formulas. Additionally, ANNs are considered black-box models, making their predictions difficult to interpret and trace.

Table 1. Key differences between mathematical-based models and ANNs.

Feature	Mathematical Cell Models	Artificial Neural Networks
Estimation approach	Use predefined equations based on battery models.	Require training on historical data to develop a model and estimate SOC.
Training requirement	None (parameters are predefined), although a fitting process is required to parameterize the model.	Require high-quality datasets for training.
Computational complexity	Electrochemical models: high. Impedance FOMs: medium. Electrical ECMs: low.	High computational demand, risk of overfitting, and convergence issues during training.
Flexibility and generalization capability	Limited (depends on model assumptions).	High (adaptive to different battery conditions, and can benefit from transfer learning).
Real-time feasibility	PDE-based: no. ODE-based: yes.	May require optimization for implementation in on-board BMSs.

2.4.3. Support Vector Machines

Support vector machines or support vector regression (SVR) techniques aim to identify the optimal hyperplane in a high-dimensional space that best represents the relationship between the input variables $\{x_1, x_2, \ldots, x_N\}$, and the actual output values of the system

$\{y_1, y_2, \ldots, y_N\}$ for N samples in the training set [92]. For example, the vector $\boldsymbol{x}$ can include the following variables: current, voltage and temperature measurements. Transformations or kernels are often used to map input features into a higher-dimensional space, allowing the algorithm to capture complex, nonlinear relationships. Figure 11 illustrates how data that are linearly inseparable in the input space are mapped to a separable output space using kernels.

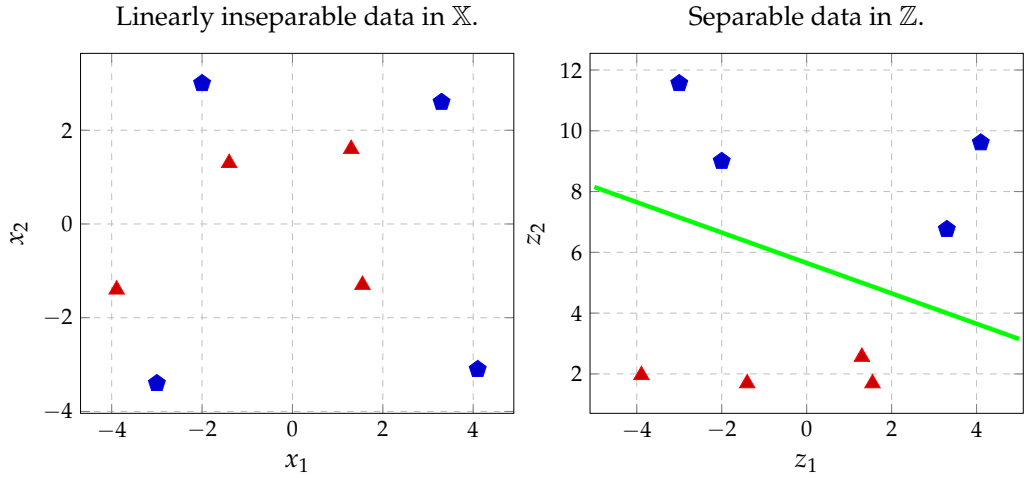

Figure 11. Mapping input data to a new feature space ($\mathbb{Z}$), $\mathbb{Z} = K(\mathbb{X})$, using the kernel $K(x_1, x_2) = (x_1, x_2 \cdot x_2)$.

The ε-SVR method (unlike traditional linear regression models that use the MSE as loss function for optimization) tries to find the function $f(\boldsymbol{x})$ that best approximates the data allowing for some deviations within a specific margin ε [92]. Therefore, the algorithm tries to find a function that captures the underlying patterns in the data and at the same time it allows a controlled level of deviation [93], increasing robustness against noise.

To make estimates using linear regression, the equation $f(\boldsymbol{x}) = \langle \boldsymbol{w}, \boldsymbol{x} \rangle + b$ is employed [92]. In this expression $\langle \cdot, \cdot \rangle$ denotes the dot product in the input space, $\boldsymbol{w}$ is a weight vector with a dimension equal to that of the input space and a direction perpendicular to the hyperplane that separates both datasets, and the parameter b is the offset or distance of the hyperplane from the origin along the normal vector $\boldsymbol{w}$. To avoid overfitting, the function $f(\boldsymbol{x})$ should be as smooth as possible, which is achieved by minimizing the norm of $\boldsymbol{w}$ to keep it small. This optimization assumes that $f(\boldsymbol{x})$ can approximate all pairs $\{\boldsymbol{x}_i, y_i\}$ with ε accuracy. However, when noise or outliers prevent this level of accuracy, a penalty (represented by the slack variables ξ_i and ξ_i^*) is assigned to these outliers (see Figure 12).

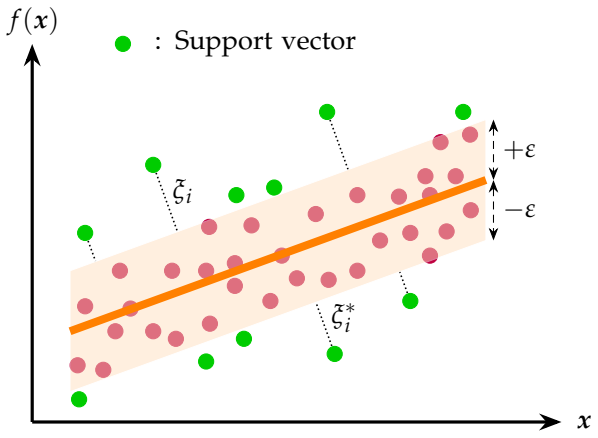

Figure 12. The ε-SVR method looks for a function that approximates the data, allowing certain deviations within a defined range ε.

The resulting optimization problem can then be formulated as follows [92]:

$$\text{Minimize:} \quad \frac{1}{2}||\boldsymbol{w}||^2 + C\sum_{i=1}^{N}(\xi_i + \xi_i^*) \tag{16}$$

$$\text{Constraints:} \quad y_i - \langle \boldsymbol{w}, \boldsymbol{x}_i \rangle - b \leq \varepsilon + \xi_i \tag{17}$$

$$\langle \boldsymbol{w}, \boldsymbol{x}_i \rangle + b - y_i \leq \varepsilon + \xi_i^* \tag{18}$$

$$\xi_i, \xi_i^* \geq 0 \tag{19}$$

The constant $C > 0$ controls the trade-off between the smoothness of the function $f(\boldsymbol{x})$ and minimizing the total error (the sum of the slack variables) [94].

Summing up, the implementation of SVR for SOC estimation begins with preparing the time-series data, which can include features like past SOC values, voltage, current, and temperature. These data are typically split into a training set for learning the model and a test set for validation. Feature scaling or normalization is often performed to ensure that all variables contribute equally to the model. Next, a kernel is selected to transform the input data into a higher-dimensional space. Common kernels are linear, polynomial, or radial basis function, with the radial basis function kernel often being preferred for its ability to model nonlinear relationships.

Once the kernel is chosen, the SVR model is trained on the historical data to learn a regression function that maximizes the margin between predicted and actual SOC values, while allowing for some error. Support vectors directly influence the model's predictions. Key hyperparameters, such as the regularization parameter (C) and margin (ε), are tuned to optimize the model's performance. After training, for time-series data such as SOC, the model can be further enhanced by incorporating lagged features into the input, enabling the model to capture temporal dependencies.

Two articles using SVMs for state-of-charge estimation are now reviewed. An improved grey wolf algorithm was used in [93] to optimize an SVM model, with voltage, current, and temperature as inputs and a Gaussian kernel for transformation. This model achieved maximum absolute errors below 2% in estimating the SOC of lithium-ion batteries during discharge. In [95], voltage, current, and temperature were also used as inputs, but a genetic algorithm served as the optimizer, paired with a radial basis function kernel. The optimized parameters, $C = 1100$ and $\varepsilon = 0.0002$, led to maximum relative errors under 3%.

In summary, SVM-based estimation methods are generally less prone to overfitting. The training process relies on convex optimization, which ensures convergence to a global minimum and avoids the local minima issues common in ANNs [92]. However, SVMs tend to perform best when the training data are limited. For larger datasets or highly complex relationships, SVMs may require substantial computational resources and may struggle to capture intricate, nonlinear dependencies without extensive tuning, which can limit their flexibility compared to some data-driven models.

2.4.4. Fusion Models for Battery State-of-Charge Estimation

Given the flexibility and wide-ranging applications demonstrated by data-driven methods, particularly ANNs, this subsection explores three studies where ANNs are coupled with mathematical model-based approaches or the Coulomb counting method. These hybrid models aim to enhance modeling capabilities, notably improving terminal voltage and SOC estimation accuracy.

In [96], a novel SOC estimation approach was proposed to accurately capture battery behavior across a wide temperature range and the full SOC spectrum. A Thevenin ECM was employed to reduce computational complexity, while a CNN was used to develop the ANN-based model to predict terminal voltage by learning the relationship between battery

inputs and outputs. The CNN utilized the current I_k, temperature T_k, and the previous voltage U_{k-1} and SOC_{k-1} as inputs.

The proposed multi-model fusion method integrated the SOC as the state vector x_{k+1} and combined the outputs of the Thevenin model and the CNN to generate a fused estimate of terminal voltage (see Figure 13). The mathematical representation of this fusion is presented in the general state-space equations outlined below:

$$x_{k+1} = SOC_{k+1} = SOC_k + \frac{\eta I_k \Delta t}{Q} \tag{20}$$

$$\begin{aligned} y_k &= U_{fusion}(I_k, SOC_k, T_k, U_{k-1}) \\ &= \omega m_1 \cdot U_{ECM} + \omega m_2 \cdot U_{CNN}(I_k, SOC_k, T_k, U_{k-1}) \end{aligned} \tag{21}$$

where U_{ECM} and U_{CNN} represent the voltages estimated by the ECM and CNN [96], respectively. The weights of each model, ωm_1 and ωm_2, which depend on SOC and temperature, were initially calculated offline using the standard deviation weight assignment method. However, to address the challenges posed by variations in ECM parameters and SOC/temperature-dependent weights due to changes in working conditions in electric vehicle applications, an adaptive weight correction method was implemented. This method corrects the weights dynamically whenever the error of the ECM or CNN exceeds 0.05 V. Furthermore, a multi-algorithm framework was adopted, combining the UKF, central difference Kalman filter (CDKF), and Cubature Kalman filter (CKF) to mitigate the individual limitations of each algorithm and enhance overall error compensation.

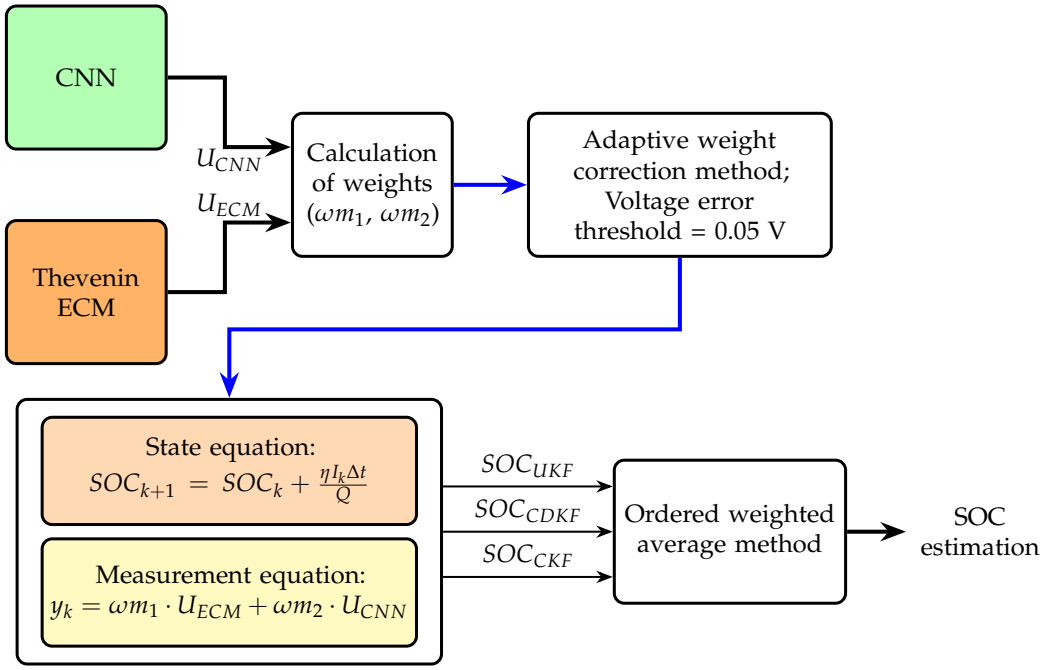

Figure 13. SOC estimation strategy adopted in [96].

The adaptive weight correction multi-algorithm fusion model was tested under the Beijing Dynamic Stress Test (BJDST), DST, FUDS, UDDS, and SFTP driving profiles at various temperatures (10 °C, 20 °C, 30 °C, and 40 °C). It achieved a maximum error of 150 mV across the entire SOC range and RMS errors within 18 mV, demonstrating its ability to accurately predict battery terminal voltages across different temperatures, even at low SOC levels.

Additionally, SOC estimation was evaluated at 20 °C under UDDS and DST conditions, achieving SOC estimation errors within 1%. The proposed method was further validated with a 10% error in the initial SOC, showing excellent traceability by converging to the true SOC within 600 s, with RMS error and MAE values below 0.004 and 0.01, respectively.

In [97], a closed-loop framework (see Figure 14) was proposed for SOC estimation in hierarchical scenarios, integrating a deep CNN with a maximum correntropy square-root Cubature Kalman filter (MCSCKF). The deep CNN was designed to model the relationship between SOC and the measurement equation of the Kalman filter, while the MCSCKF enhanced performance in the presence of non-Gaussian noise.

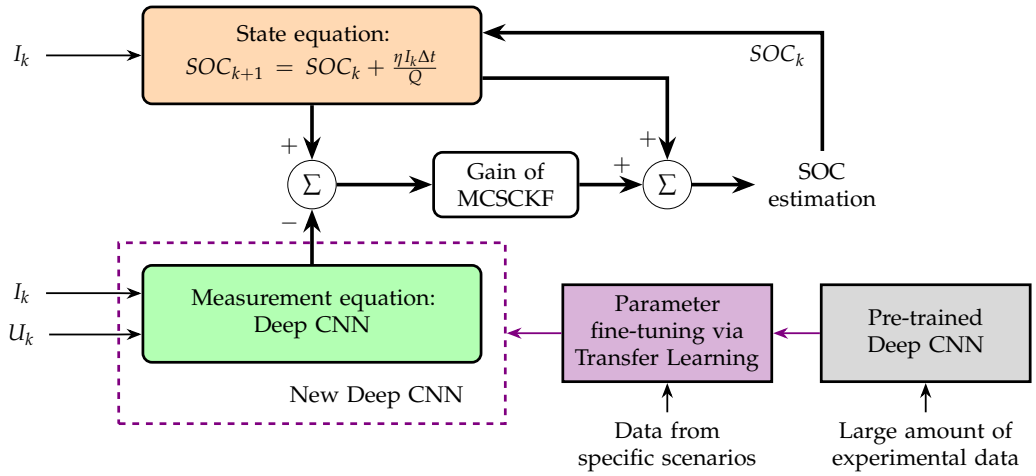

Figure 14. SOC estimation framework from [97] and transfer learning approach.

The deep CNN architecture consisted of an input layer, three two-dimensional (2D) convolutional layers, three ReLU activation layers, two average pooling layers, two fully connected layers, and a regression layer. This multi-layer CNN structure enabled the first convolutional layer to extract basic common features, while the final convolutional layer captured complex, application-specific information. The model utilized only voltage and current as inputs to the deep CNN, with the measurement equation for the Kalman filter defined as follows [97]:

$$y_k = f_{DCNN}((U_{k-L}, \ldots, U_k), (I_{k-L}, \ldots, I_k)) + v_k \tag{22}$$

where f_{DCNN} represents the computation performed by the deep CNN, L denotes the length of the moving window, U_k and I_k are the voltage and current, respectively, and v_k is the measurement noise. The state equation is identical to Equation (20), with the Coulombic efficiency (η) set to one. To further enhance adaptability, transfer learning was employed, fine-tuning the last few layers of the pre-trained model to suit specific application scenarios.

The proposed framework was evaluated in three hierarchical scenarios using datasets from three types of lithium-ion batteries with different capacity ratings, nominal voltages, discharge voltages, and internal impedances. The evaluation led to the following conclusions:

1. In Scenario 1, where the same type of batteries as the pre-trained model were used, transfer learning was not required. The field model achieved an RMS error of 0.86% and an MAE of 0.71%;
2. In Scenario 2, involving different types of batteries from the pre-trained model, transfer learning was applied. For ternary lithium batteries, the field model achieved an RMS error of 0.55% and an MAE of 0.42%. In contrast, for $LiFePO_4$ batteries, the field model recorded an RMS error of 2.29% and an MAE of 1.60%;

3. In Scenario 3, where different types of aged batteries were used as the pre-trained model, only the fully connected layers were fine-tuned. For aged ternary lithium batteries, the SOC estimation achieved an RMS error of 0.72% and an MAE of 0.56%. For aged $LiFePO_4$ batteries, the SOC estimation recorded an RMS error of 2.26% and an MAE of 1.78%.

Finally, in [98], a fusion framework was proposed, combining Deep Learning with a Kalman filter (see Figure 15). The data-driven component utilized an encoder–decoder architecture with attention mechanisms integrated into a CNN-LSTM model, enabling the efficient extraction of comprehensive information across both spatial and temporal scales.

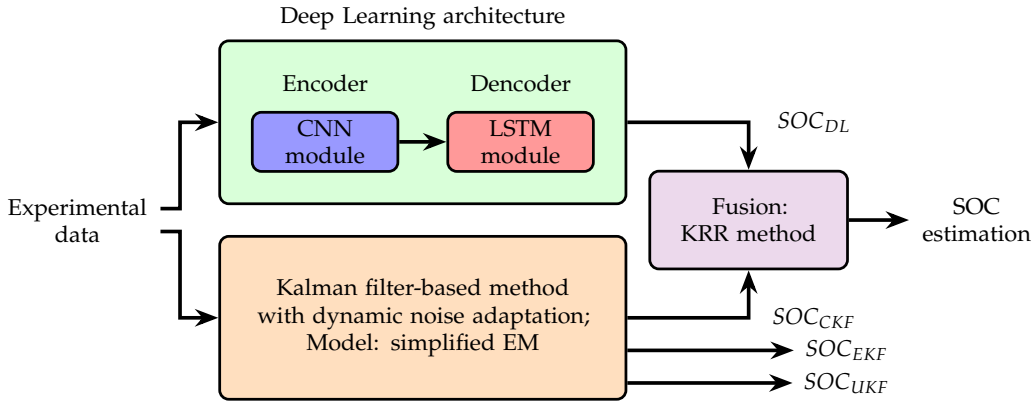

Figure 15. SOC estimation approach proposed in [98], combining a CNN-LSTM architecture and a Kalman filter.

In the filter-based stage, it was recognized that the process and measurement noises depend on the dynamic state and actual operating environment. Using constant noise values could lead to reduced accuracy or even filter divergence. To address this, an adaptive law was proposed, allowing the process and measurement noises to be dynamically adjusted following the correction phase. This resulted in adaptive nonlinear versions of the EKF, UKF, and CKF.

The filtering stage operated on a simplified EM that captured the battery's internal mechanisms, divided into five key processes: basic working, solid-phase diffusion, liquid-phase diffusion, reaction polarization, and ohmic polarization. Finally, the proposed fusion method, employing parallel structures, combined the SOC values estimated by both the Deep Learning and filter-based approaches, mathematically expressed as follows [98]:

$$SOC_{DF} = f_{DF}(SOC_{DL}, SOC_{KF}) \tag{23}$$

where f_{DF} represents the data fusion function, while SOC_{DF}, SOC_{DL}, and SOC_{KF} denote the SOC estimation results obtained through the fusion method, Deep Learning, and Kalman filter, respectively. Various approaches for determining the data fusion function were evaluated, including weighted averaging, entropy weight method, ordered weighted averaging, variance minimization, probabilistic fusion, adaptive Kalman filter, and kernel ridge regression (KRR).

The Deep Learning model was trained under the FUDS condition and tested using the New European Driving Cycle (NEDC) condition. Additionally, the voltage accuracy of the simplified EM was verified, achieving MAEs of 7.7478 mV and 8.1773 mV for FUDS and NEDC, respectively. Corresponding RMS errors were 11.1058 mV and 11.3239 mV, successfully capturing the voltage behavior of the battery.

Regarding the SOC estimation accuracy of the Deep Learning, filter-based, and fusion methods, the following conclusions were drawn:

1. The Deep Learning model achieved an MAE of 0.6808% and an RMS error of 0.8663%, with the maximum absolute error remaining around 2.1%. This demonstrates that the Deep Learning stage effectively captures the temporal dependencies of SOC changes in relation to physical quantities;
2. The Kalman filter-based methods revealed that all three approaches produced results without outliers, indicating that these methods are more stable and less prone to excessive fluctuations. However, the adaptive EKF gradually showed deviations from the reference value over time;
3. All three Kalman filters demonstrated rapid convergence to the reference value. Robustness was assessed based on the time required for SOC to converge within a 1% error margin: 292 s for the adaptive EKF, 144 s for the adaptive UKF, and 67 s for the adaptive CKF, with the adaptive CKF excelling as the most robust. Additionally, the adaptive CKF showcased the best overall performance, achieving the smallest MAE and RMS errors of 0.5750% and 0.6292%, respectively, with a maximum absolute error of 1.1658%;
4. Finally, the fusion method, combining the results of the Deep Learning and adaptive CKF methods, demonstrated outstanding performance when utilizing the KRR approach (see Table 2). The KRR method effectively handled the fusion process, achieving superior results across all evaluation metrics. The MAE, RMS error, and maximum absolute error were 0.2341%, 0.3072%, and 0.7730%, respectively. These results indicate that the SOC estimation achieved by the fusion method is highly accurate, less prone to fluctuations, and exceptionally stable, establishing KRR as an effective meta-learning model for ensemble learning.

Table 2. The SOC evaluation metrics for the Deep Learning, CKF-based, and fusion methods [98].

Method	MAE (%)	RMS Error (%)	Maximum Absolute Error (%)
Deep Learning	0.6808	0.8663	2.1009
Adaptive CKF	0.5750	0.6292	1.1658
Fusion with KRR	0.2341	0.3072	0.7730

Overall, the fusion methods analyzed in [96–98] demonstrate the ability to effectively process and integrate multiple information sources, significantly reducing errors associated with individual methods and exhibiting greater adaptability to complex scenarios when estimating SOC. These characteristics highlight their advantages in forecasting and their substantial potential for implementation in on-board BMSs. In practical applications, data-driven hybrid methods can be efficiently deployed using cloud computing technologies and edge-cloud collaboration strategies [98], enabling real-time performance and scalability.

3. Summary of State-of-Charge Estimation Methods

This paper explains the fundamentals of each method and reviews the relevant state of the art to compare current results achieved in SOC estimation.

Lookup table and ampere-hour counting are straightforward and effective methods in controlled environments where frequent recalibrations can prevent error accumulation. However, these methods on their own are less suited for applications requiring robust, long-term accuracy. While these methods have inherent limitations, numerical evidence demonstrates their potential under specific conditions. For instance, [40] showed that

combining ampere-hour counting with periodic updates using OCV lookup tables after one-hour rest periods resulted in absolute SOC estimation errors below 3%.

Electrochemical models offer highly accurate characterization of internal cell processes, but their complexity requires substantial processing power to solve the equations involved. Despite this, their potential is evident in numerical evaluations, where errors as low as 0.5% for SOC estimation and below 1% for lithium concentration were achieved using Kalman filter-based observers.

Equivalent circuit models provide a balance between accuracy, robustness, and computational cost when estimating SOC. However, equivalent circuit models do not have the ability to predict internal processes and cell degradation, and they are limited to contexts similar to those in which the data for parameterization were collected. Numerical evaluations highlight their accuracy, with errors as low as 0.61% using advanced observers such as the UKF and particle filters, and less than 3% when using EKF-based estimation.

The electrochemical impedance models based on impedance spectroscopy describe the cell's behavior across a wide frequency range, but their use in the automotive sector is constrained by the high cost of the required equipment for in-vehicle installation. Studies highlight their potential accuracy; for example, in [67], combining impedance data with conventional inputs like voltage, current, and temperature, and employing Machine Learning techniques such as SVMs, yielded RMS errors as low as 1.06% at 100 mHz and 1.09% at 100 Hz. On the other hand, FOMs have shown strong generalization capabilities when tested across different cells, making them a valuable solution for reducing computational overhead in BMSs tasked with monitoring thousands of cells. Furthermore, [68] highlights the robustness of FOMs against temperature variations as well as voltage and current sensor drifts. However, the truncation error introduced by the short-memory principle violates the Kalman filter assumption that errors are white noise, which may adversely affect SOC estimation accuracy [68].

Data-driven approaches rely on Machine Learning platforms to optimize network parameters. These models excel at learning complex patterns, making them highly versatile tools, especially with the vast amounts of data available today.

Fuzzy logic models are well suited for environments with uncertain or imprecise information, as they follow a set of human-understandable rules. Among the disadvantages, we can point out its limited learning capability because fuzzy systems do not inherently "learn" from data; rule sets need to be crafted or optimized manually. Moreover, for complex systems, the number of rules can grow substantially, making the model cumbersome to manage and less efficient. Fuzzy logic approaches have achieved SOC estimation errors ranging from approximately 0.5% to 5% in studies using experimental setups for lead-acid, lithium-ion, and NiMH batteries [79–81]. However, some setups such as those relying on current, voltage, and temperature measurements as inputs for the fuzzy logic model, reported higher maximum errors of up to 10% [83].

Neural networks can automatically learn relevant features from raw data, often reducing the need for extensive feature engineering. On the other hand, training neural networks demand substantial processing power and time, especially in deep networks. Furthermore, careful attention should be given to the optimization mechanism during the training phase to ensure proper convergence and mitigate the risk of overfitting. Neural networks have achieved errors typically under 10% when estimating the SOC. Optimized architectures, such as genetic algorithm-enhanced feedforward networks, reduced errors further, achieving average errors as low as 0.9% on training data but with maximum errors up to 13% in validation [89]. Advanced models like bidirectional LSTM and GRU networks achieved RMS errors below 4.67% and 0.83%, respectively, with the GRU network excelling in dynamic drive cycles and varying temperatures [90,91].

Support vector machines perform well with a large number of features, making them especially effective in high-dimensional spaces. However, support vector machines exhibit difficulty with highly nonlinear data. SVM models have demonstrated good accuracy when estimating the SOC of lithium-ion cells; one approach using a grey wolf optimizer achieved maximum absolute errors below 2%, while another employing a genetic algorithm with a radial basis function kernel reported maximum relative errors under 3% [93,95].

Finally, fusion or hybrid approaches enable the integration of the strengths of both data-driven methods and mathematical-based models while compensating for their individual weaknesses. The analyzed hybrid methods have demonstrated strong SOC estimation capabilities, incorporating weight correction and noise adaptation mechanisms [96,98]. Moreover, data-driven hybrid methods can benefit from transfer learning by repurposing pre-trained models or networks to address different scenarios [97].

Tables 3 and 4 present a comparison of the advantages and challenges of the OCV, Coulomb counting, mathematical-based, and data-driven methods analyzed.

Table 3. Comparison of advantages and challenges of OCV, Coulomb counting, and mathematical-based SOC estimation methods.

Method	Advantages	Challenges
Open-circuit voltage	• High accuracy under equilibrium conditions. • Non-intrusive; can be measured without disturbing battery operation. • Simple implementation; requires only voltage measurement and a pre-established OCV-SOC curve.	• Requires the battery to rest for a long period to reach equilibrium. • The OCV-SOC curve varies with temperature, reducing accuracy if temperature effects are not compensated. • Not practical for dynamic SOC estimation during operation.
Coulomb counting	• Easy implementation. • Can track SOC dynamically during battery operation without requiring rest periods. • Provides fine-grained SOC updates since it continuously integrates current.	• Highly dependent on precise current measurements; sensor noise can degrade accuracy. • Requires an accurate initial SOC value; otherwise, all future calculations will be offset. • Self-discharge is not accounted for, which can cause SOC estimation errors in long idle periods.
Electrochemical models	• Provide highly accurate SOC estimations by capturing the internal electrochemical behavior of the battery. • Account for key internal dynamics, including ion transport, reaction kinetics, and temperature effects.	• Solving PDEs requires significant computational resources. • Requires extensive parameter extraction and lab testing to build an accurate model. • Not practical for real-time estimation.
Electrical equivalent circuit models	• Provide a good trade-off between accuracy and computational efficiency. • Model parameters can be determined through experimental techniques such as pulse discharge tests. • Can be implemented in real-time applications due to their relatively simple mathematical structure.	• Do not fully capture electrochemical phenomena such as diffusion effects and side reactions. • Are constrained to operating conditions similar to those used for parameterization.
Electrochemical impedance models	• More accurately model internal resistances and capacitances compared to electrical ECMs. • Can track battery aging and degradation by analyzing impedance variations over time.	• Impedance measurements are very sensitive to noise and require precise instrumentation. • The high cost of impedance spectroscopy equipment limits their adoption for SOC estimation in electric vehicles.

Table 4. Comparison of advantages and challenges of fuzzy logic, ANN, and SVM methods.

Method	Advantages	Challenges
Fuzzy logic	• Handles imprecise and uncertain measurements effectively, making it suitable for real-world battery conditions. • Allows the inclusion of human expertise in defining SOC estimation rules, improving adaptability. • Requires fewer resources compared to other Machine Learning methods.	• As the number of input variables grows, defining and tuning fuzzy rules becomes more complex. • The accuracy of the model relies on well-defined membership functions and rules, which require domain expertise. • Lower accuracy in highly nonlinear systems.
Artificial neural networks	• Capable of capturing complex nonlinear relationships between input variables and SOC. • Can adapt to varying battery conditions and dynamic operating environments through training. • Can improve over time as more data become available, enhancing performance with experience.	• Performance is heavily dependent on the availability of high-quality, diverse training data. • Selecting the appropriate network architecture, learning rate, and other hyperparameters requires careful optimization and expertise. • If not properly regularized or validated, ANNs can overfit to training data, reducing generalization to unseen data.
Support vector machines	• Offer good generalization capabilities, especially when used with kernel methods, preventing overfitting. • Handle high-dimensional feature spaces effectively, which is useful when incorporating multiple variables for SOC estimation. • Can achieve good performance with relatively smaller datasets, which is useful when data are limited.	• Finding the optimal set of hyperparameters requires significant effort and computational resources. • Can struggle with very large datasets or complex kernel functions.

Table 5 outlines the primary applications where the analyzed methods are most effective, providing insights into their practical use cases.

Table 5. Specific applications of analyzed SOC estimation methods for optimal effectiveness.

Method	Applications
Open-circuit voltage	• Used in controlled conditions or lab settings to study battery behavior and create accurate SOC reference curves.
Coulomb counting	• Used in combination with other methods to track SOC. • Commonly integrated in BMSs to provide continuous SOC estimation in real-time.
Electrochemical models	• Used in laboratories to study battery behavior and develop new battery chemistries. • Ideal in high-precision simulations where understanding the exact cause and effect of transport kinetics is crucial.
Electrical and impedance-based models	• Commonly used in on-board BMSs for online SOC estimation, balancing accuracy and computational efficiency for dynamic driving conditions.
Data-driven methods	• Applied in situations where a high degree of nonlinearity exists, and the model needs to quickly adapt to varied conditions.

4. Conclusions, Future Work, and Research Perspectives

Through an extensive analysis of the commonly used SOC estimation methods, we identified that each approach has distinct strengths and limitations, and each one of them performs well under specific conditions.

Most studies assess the precision of SOC estimation methods exclusively in offline, simulated environments using computer-aided tools, lacking physical implementations programmed on microcontrollers to achieve real-time SOC estimation. This limitation complicates the selection of an optimal estimator, as there is no concrete evidence regarding the following: (1) the number of floating-point operations needed to execute complex methods without delays, and (2) the impact of rounding errors on the accuracy of the final SOC estimation.

Furthermore, the "true" SOC often used for comparison or validation inherently contains error, as it cannot be directly measured. The closest approximation to a real SOC (excluding highly complex electrochemical models that cannot be used in real-time applications) is typically derived in laboratory or controlled environments using a Coulomb counting method with highly accurate current sensors. Consequently, the results of any SOC estimation method are often compared to a "true" SOC that is itself subjected to bias.

Moreover, comparing results across studies is challenging due to inconsistencies in the studied battery types and testing conditions. Papers often use diverse metrics to report error rates and rely on different datasets, including constant-current cell discharge conditions or distinct driving cycles sampled at different frequencies. Additionally, some studies attempt to estimate SOC using inputs that are more easily obtained in laboratory settings, without considering the challenges of acquiring such variables during real-time operation in electric vehicles. For example, [88] proposed using three cell-specific temperatures as inputs to the neural network model to estimate SOC, requiring three temperature sensors per cell. This approach is impractical for real-world applications, as battery packs typically consist of over a hundred cells.

We conclude that hybrid strategies, which combine multiple estimation methods to leverage their complementary strengths, are promising approaches. For example, integrating a neural network with the ESC cell model could provide a significant advantage in accurately estimating the SOC across different driving profiles. This highlights the need for a dedicated testing platform to implement and evaluate experimentally various SOC estimation strategies under uniform conditions, enabling a more reliable comparison of their performance. This platform will be detailed later in the section.

Building on the discussion of SOC estimation methods for individual cells, it is important to address their limitations when applied to the large-scale battery packs of electric vehicles, which often comprise hundreds of cells. The methods analyzed primarily focus on single-cell SOC estimation and do not address how to determine the SOC of an entire battery pack. Furthermore, the SOC of a battery pack currently lacks a universally accepted definition. According to [99], battery pack SOC estimation algorithms can be categorized into four types: (1) individual cell estimation, (2) lumped cell estimation, (3) reference cell estimation, and (4) mean cell and difference estimation. Among these, individual cell and reference cell estimation stand out as the most computationally intensive yet robust methods, as they effectively mitigate the impact of aging on the weakest cell in the battery pack. The SOC estimation for lithium-ion battery packs is complex due to inherent inconsistencies in cell characteristics such as capacity, internal resistance, and temperature. These inconsistencies arise from manufacturing tolerances, welding processes, and operational conditions, and they tend to grow over the battery pack's life due to non-uniform aging and thermal variations [99].

These challenges highlight the necessity of implementing effective cell balancing or equalization algorithms in battery packs. As a future step, following the evaluation of

various SOC estimation methods on a test bench, which is currently under development in our laboratory, an active battery equalizer will be designed to mitigate SOC imbalances within the battery pack. This step is critical for ensuring efficient and reliable operation. The experimental setup will monitor five battery modules connected in series (see Figure 16a), enabling the testing of different equalization algorithms. The system will dynamically identify the module with the highest SOC and the one with the lowest, using a DC/DC converter to transfer energy from the most charged module to the least charged, actively balancing the entire pack [100].

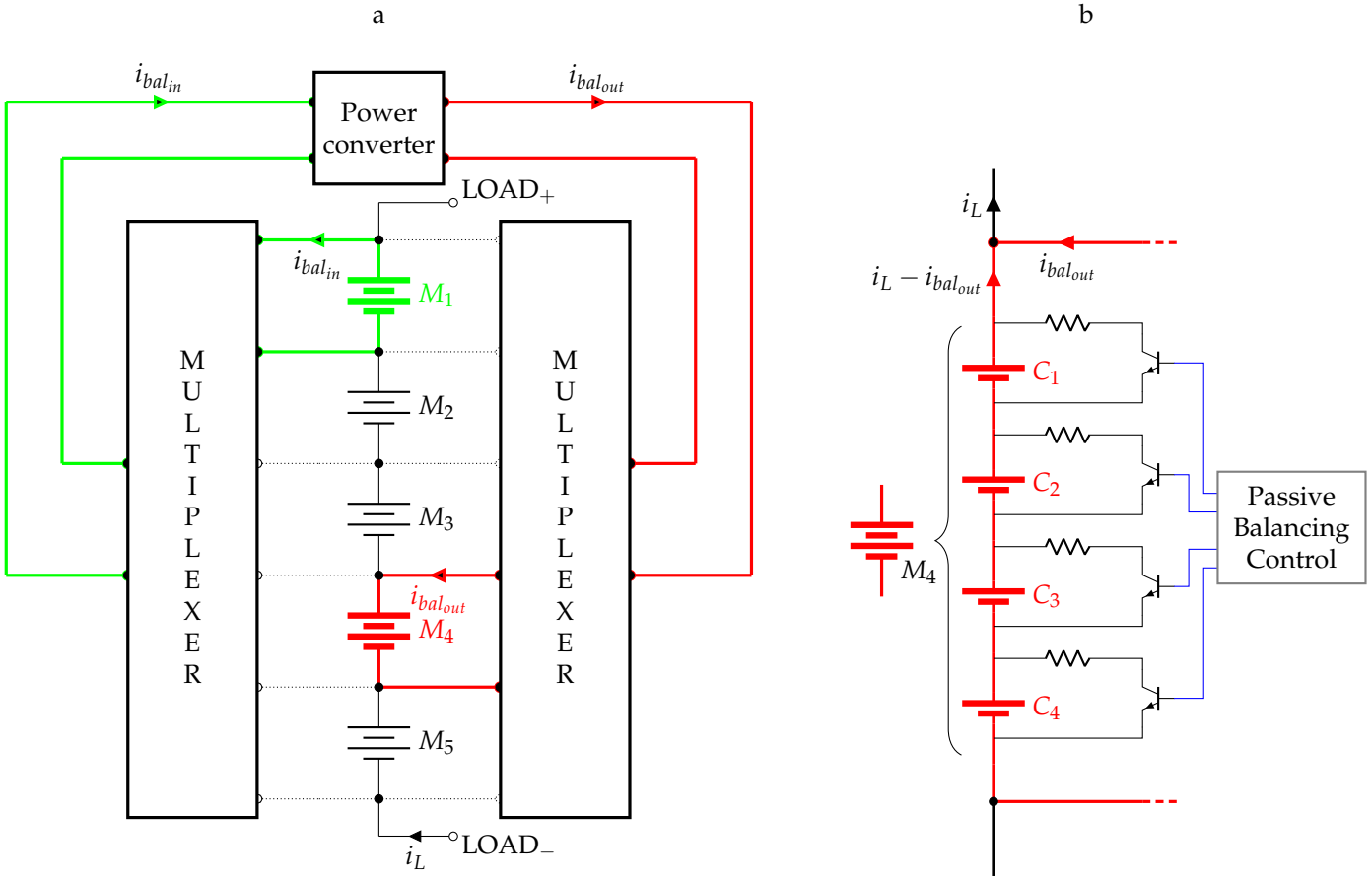

Figure 16. (**a**) Illustration of the equalizer platform transferring energy from module M_1 (highest SOC) to module M_4 (lowest SOC) [100]. (**b**) Internal structure of each battery module, including its corresponding passive balancing system.

Each of the five modules consists of four cells (see Figure 16b), automatically balanced using a traditional passive BMS. This hybrid balancing system aims to enhance performance compared to fully passive balancing strategies commonly used in vehicle battery packs, while maintaining cost-effectiveness by focusing on module-level balancing instead of cell-level balancing for the entire pack. The proposed five-module system serves as a proof of concept for potential electric vehicle applications.

Research Perspectives

After establishing that SOC estimation methods are a critical foundation for on-board applications, significant progress is still required to develop robust BMSs. One essential step forward is the integration of advanced SOH estimation and fault-diagnosis techniques into modern BMSs.

Regarding SOH estimation, traditional approaches such as capacity tests and impedance measurements often encounter limitations, including high costs, testing com-

plexity, and challenges in real-time applicability. To overcome these issues, data-driven methods have emerged as a promising alternative. Leveraging large publicly available datasets, such as those from NASA, CALCE, and Stanford-MIT, researchers can develop and validate effective SOH estimation models. These data-driven approaches utilize Machine Learning techniques (such as ANN, Gaussian process regression, and random forests [101]) alongside feature extraction methods like differential voltage/incremental capacity curves and differential temperature analysis. These methods excel in identifying complex, nonlinear patterns in battery behavior, enabling precise SOH predictions.

Furthermore, with the increasing volume of data being collected daily, data-driven methods hold great promise for transfer learning [15], enabling model generalization across various battery types while addressing data quality concerns. This trend also aligns with the development of hybrid models and domain adaptation techniques, which enhance the accuracy and robustness of SOH estimation frameworks.

Supporting this perspective, Ref. [101] presented an insightful study evaluating several data-driven models, including LSTM networks, CNN, Gaussian process regression, random forests, and transfer learning. These models were tested on a dataset of batteries with cycle lives ranging from 326 to 1266 cycles and varying degradation levels. The results revealed that the accuracy of SOH estimation models is heavily influenced by the battery's degradation protocol. This finding underscores the need for more comprehensive studies to address such variability and further improve the reliability of SOH and SOC estimation techniques.

Equally as important as the accurate estimation of SOC and SOH is the development of advanced and intelligent fault-diagnosis algorithms for the early detection of battery faults. Lithium-ion batteries operate within a narrow temperature range, making them vulnerable to thermal runaway under conditions such as overheating, overcharging, over-discharging, or mechanical damage [102]. Incidents such as electric vehicles catching fire after collisions and battery pack deformations, or even during charging at stations, underscore the critical need for robust fault-diagnosis strategies to ensure user safety and product reliability.

In [102], several fault-diagnosis methods are discussed, which can be seamlessly integrated into BMSs. For instance, one fault-detection method involves continuously comparing parameters or estimations, with measured data or reference values. If the deviation exceeds a predefined threshold, a fault alarm is triggered. This highlights the necessity of a robust and accurate battery model capable of estimating critical metrics like SOC, SOH, and terminal voltage.

However, in electric vehicle applications, multiple faults may occur simultaneously, necessitating also fault-identification methods that can address such complexities. For example, (1) hardware redundancy achieves fault isolation through the implementation of redundant sensors, ensuring that critical data remain reliable even in the presence of sensor failures, and (2) analytical redundancy utilizes a bank of subsystems, each designed to be sensitive to specific faults while remaining insensitive to others, providing a systematic way to isolate and identify multiple faults.

These strategies further emphasize the importance of accurate and well-constructed battery models. Fault diagnosis, without a doubt, is a complementary area of research to SOC and SOH estimation, offering substantial benefits to the development of safer, more reliable, and intelligent BMSs.

Author Contributions: Methodology, D.G.E. and H.V.B.; writing—original draft preparation, M.A.P.O.; writing—review and editing, M.A.P.O., D.G.E. and H.V.B. All authors have read and agreed to the published version of the manuscript.

Funding: This research was funded by the Ministry of Science and Innovation of Spain, grant number PID2023-150839OB-I00. This work was also financially supported by the Tarragona Deputation.

Data Availability Statement: No new data were created or analyzed in this study. Data sharing is not applicable to this article.

Conflicts of Interest: The authors declare no conflicts of interest.

Abbreviations

ANFIS	adaptive neuro-fuzzy inference system 16
ANN	artificial neural networks 3, 14, 17–19, 21, 30
BJDST	Beijing Dynamic Stress Test 22
BMS	battery management system 2, 9–11, 13, 14, 25, 26, 30, 32
CDKF	central difference Kalman filter 22
CKF	Cubature Kalman filter 22–24
CNN	convolutional neural networks 17, 21–23, 31
CPEs	constant phase elements 11, 14
DST	Dynamic Stress Test 13, 18, 22
ECM	equivalent circuit models 3, 8–11, 21, 22
EIM	electrochemical impedance models 11
EIS	electrochemical impedance spectroscopy 10
EKF	extended Kalman filter 10, 23–25
EM	electrochemical models 3, 6, 8, 10, 11, 23, 24
ESC	enhanced self-correcting 9, 10, 29
ESR	equivalent series resistance 12
FNN	feedforward neural networks 17, 18
FOMs	fractional-order models 8, 10–14, 25, 26
FUDS	Federal Urban Driving Schedule 10, 13, 18, 22, 24
GRU	gated recurrent unit 17, 18, 26
HWFET	Highway Fuel Economy Test 18
KRR	kernel ridge regression 24, 25
LSTM	long short-term memory 17, 18, 23, 26, 31
MAE	mean-absolute error 13, 16, 22–25
MCSCKF	maximum correntropy square-root Cubature Kalman filter 22
MSE	mean-squared error 10, 19
NEDC	New European Driving Cycle 24
NiCd	nickel cadmium 7
NiMH	nickel–metal hydride 4, 7, 9, 15, 26
OCV	open-circuit voltage 2–5, 9, 25, 26
ODEs	ordinary differential equations 9, 10
PDEs	partial differential equations 6–8
PDF	probability density function 11
ReLU	rectified linear unit 17, 22
RMS	root-mean-squared 10, 11, 13, 16, 18, 22–26
RNN	recurrent neural networks 17, 18
SEI	solid electrolyte interphase 2, 12
SFTP	Supplemental Federal Test Procedures 18, 22
SOC	state-of-charge 1–6, 8–18, 20–26, 29–32
SOH	state of health 1–3, 17, 30–32
SOP	state of power 1–3
SVM	support vector machines 11, 21, 25, 26
SVR	support vector regression 19–21
UCDS	Unified Cycle Driving Schedule 18
UDDS	Urban Dynamometer Driving Schedule 10, 13, 18, 22
UKF	unscented Kalman filter 10, 13, 22–25

References

1. Al-Ghussain, L.; Darwish Ahmad, A.; Abubaker, A.M.; Mohamed, M.A. An integrated photovoltaic/wind/biomass and hybrid energy storage systems towards 100 percent renewable energy microgrids in university campuses. *Sustain. Energy Technol. Assess.* **2021**, *46*, 101273. [CrossRef]
2. Akinlabi, A.H.; Solyali, D. Configuration, design, and optimization of air-cooled battery thermal management system for electric vehicles: A review. *Renew. Sustain. Energy Rev.* **2020**, *125*, 109815. [CrossRef]
3. Li, M.; Lu, J.; Chen, Z.; Amine, K. 30 Years of Lithium-Ion Batteries. *Adv. Mater.* **2018**, *30*, 1800561. [CrossRef]
4. Plett, G.L. *Battery Management Systems, Volume I: Battery Modeling*; Artech House Power Engineering and Power Electronics; Artech House: Washington, DC, USA, 2015.
5. Wang, Z.; Feng, G.; Zhen, D.; Gu, F.; Ball, A. A review on online state of charge and state of health estimation for lithium-ion batteries in electric vehicles. *Energy Rep.* **2021**, *7*, 5141–5161. [CrossRef]
6. Ye, Y.; Chou, L.Y.; Liu, Y.; Wang, H.; Lee, H.; Huang, W.; Wan, J.; Liu, K.; Zhou, G.; Yang, Y.; et al. Ultralight and fire-extinguishing current collectors for high-energy and high-safety lithium-ion batteries. *Nat. Energy* **2020**, *5*, 786–793. [CrossRef]
7. Xiong, R.; Cao, J.; Yu, Q.; He, H.; Sun, F. Critical Review on the Battery State of Charge Estimation Methods for Electric Vehicles. *IEEE Access* **2018**, *6*, 1832–1843. [CrossRef]
8. Huang, Z.; Zhao, C.; Li, H.; Peng, W.; Zhang, Z.; Wang, Q. Experimental study on thermal runaway and its propagation in the large format lithium ion battery module with two electrical connection modes. *Energy* **2020**, *205*, 117906. [CrossRef]
9. Wu, M.; Qin, L.; Wu, G. State of power estimation of power lithium-ion battery based on an equivalent circuit model. *J. Energy Storage* **2022**, *51*, 104538. [CrossRef]
10. Xiong, R.; Li, L.; Tian, J. Towards a smarter battery management system: A critical review on battery state of health monitoring methods. *J. Power Sources* **2018**, *405*, 18–29. [CrossRef]
11. Guo, R.; Shen, W. Recent advancements in battery state of power estimation technology: A comprehensive overview and error source analysis. *J. Energy Storage* **2024**, *103*, 114294. [CrossRef]
12. Thingvad, M.; Calearo, L.; Thingvad, A.; Viskinde, R.; Marinelli, M. Characterization of NMC Lithium-ion Battery Degradation for Improved Online State Estimation. In Proceedings of the 2020 55th International Universities Power Engineering Conference (UPEC), Torino, Italy, 1–4 September 2020; pp. 1–6. [CrossRef]
13. Anseán, D.; García, V.M.; González, M.; Blanco-Viejo, C.; Viera, J.C.; Pulido, Y.F.; Sánchez, L. Lithium-Ion Battery Degradation Indicators Via Incremental Capacity Analysis. *IEEE Trans. Ind. Appl.* **2019**, *55*, 2992–3002. [CrossRef]
14. Kemeny, M.; Ondrejka, P.; Mikolasek, M. Incremental Capacity Analysis (ICA) Via Galvanostatic Intermittent Titration Technique (GITT) Data For Battery Degradation Study. In Proceedings of the 2022 14th International Conference on Advanced Semiconductor Devices and Microsystems (ASDAM), Smolenice, Slovakia, 23–26 October 2022; pp. 1–4. [CrossRef]
15. Shen, L.; Li, J.; Meng, L.; Zhu, L.; Shen, H.T. Transfer Learning-based State of Charge and State of Health Estimation for Li-ion Batteries: A Review. *IEEE Trans. Transp. Electrif.* **2023**. [CrossRef]
16. Jongerden, M.; Haverkort, B. *Battery Modeling*; CTIT Report; University of Twente: Enschede, The Netherlands, 2008.
17. Li, H.; Jin, Y.; Yu, D. Online Estimation of Battery Model Parameters and State of Charge Using Dual Time-Scaled Technique Without Open Circuit Voltage Experiment. *IEEE Trans. Instrum. Meas.* **2024**, *73*, 1–13. [CrossRef]
18. Balasingam, B.; Pattipati, K.R. On the Identification of Electrical Equivalent Circuit Models Based on Noisy Measurements. *IEEE Trans. Instrum. Meas.* **2021**, *70*, 1–16. [CrossRef]
19. Khan, Z.A.; Shrivastava, P.; Amrr, S.M.; Mekhilef, S.; Algethami, A.A.; Seyedmahmoudian, M.; Stojcevski, A. A Comparative Study on Different Online State of Charge Estimation Algorithms for Lithium-Ion Batteries. *Sustainability* **2022**, *14*, 7412. [CrossRef]
20. Cui, Y.; Chen, Y. Prognostics of Lithium-Ion Batteries Based on Capacity Regeneration Analysis and Long Short-Term Memory Network. *IEEE Trans. Instrum. Meas.* **2022**, *71*, 1–13. [CrossRef]
21. Shi, Q.; Jiang, Z.; Wang, Z.; Shao, X.; He, L. State of Charge Estimation by Joint Approach With Model-Based and Data-Driven Algorithm for Lithium-Ion Battery. *IEEE Trans. Instrum. Meas.* **2022**, *71*, 1–10. [CrossRef]
22. Pattipati, B.; Balasingam, B.; Avvari, G.; Pattipati, K.; Bar-Shalom, Y. Open circuit voltage characterization of lithium-ion batteries. *J. Power Sources* **2014**, *269*, 317–333. [CrossRef]
23. Stroe, D.I.; Swierczynski, M.; Stroe, A.I.; Kær, S.K. Generalized Characterization Methodology for Performance Modelling of Lithium-Ion Batteries. *Batteries* **2016**, *2*, 37. [CrossRef]
24. Plett, G.L. *Battery Management Systems, Volume II: Equivalent-Circuit Methods*; Artech House Power Engineering and Power Electronics; Artech House: Washington, DC, USA, 2015.
25. Thele, M.; Bohlen, O.; Sauer, D.U.; Karden, E. Development of a voltage-behavior model for NiMH batteries using an impedance-based modeling concept. *J. Power Sources* **2008**, *175*, 635–643. [CrossRef]
26. García-Plaza, M.; Eloy-García Carrasco, J.; Peña-Asensio, A.; Alonso-Martínez, J.; Arnaltes Gómez, S. Hysteresis effect influence on electrochemical battery modeling. *Electr. Power Syst. Res.* **2017**, *152*, 27–35. [CrossRef]

27. Roscher, M.; Bohlen, O.; Vetter, J. OCV Hysteresis in Li-Ion Batteries including Two-Phase Transition Materials. *Int. J. Electrochem.* **2011**, *2011*, 984320. [CrossRef]
28. Kasavajjula, U.; Wang, C.; Arce, P. Discharge Model for LiFePO4 Accounting for the Solid Solution Range. *J. Electrochem. Soc.* **2008**, *155*, A866. [CrossRef]
29. Meethong, N.; Huang, H.Y.; Speakman, S.; Carter, W.; Chiang, Y.M. Strain Accommodation during Phase Transformations in Olivine-Based Cathodes as a Materials Selection Criterion for High-Power Rechargeable Batteries. *Adv. Funct. Mater.* **2007**, *17*, 1115–1123. [CrossRef]
30. Dreyer, W.; Jamnik, J.; Guhlke, C.; Huth, R.; Moskon, J.; Gaberscek, M. The thermodynamic origin of hysteresis in insertion batteries. *Nat. Mater.* **2010**, *9*, 448–453. [CrossRef]
31. Rahimi Eichi, H.; Chow, M.Y. Modeling and analysis of battery hysteresis effects. In Proceedings of the 2012 IEEE Energy Conversion Congress and Exposition (ECCE), Raleigh, NC, USA, 15–20 September 2012; pp. 4479–4486. [CrossRef]
32. Kim, T.; Qiao, W.; Qu, L. An Enhanced Hybrid Battery Model. *IEEE Trans. Energy Convers.* **2019**, *34*, 1848–1858. [CrossRef]
33. Jiang, J.; Zhang, C. *Fundamentals and Applications of Lithium-Ion Batteries in Electric Drive Vehicles*; John Wiley & Sons: Hoboken, NJ, USA, 2015.
34. Khamari, S.; Gaikwad, A.; Patil, A.; Argade, S.; Mulla, A. Passive Cell Equalization and State of Charge Estimation Using Coulomb Counting Approach. In Proceedings of the 2023 Global Conference on Information Technologies and Communications (GCITC), Bangalore, India, 1–3 December 2023; pp. 1–6. [CrossRef]
35. Zode, P.; Shankaran, V.; Bilurkar, P. Temperature Dependent Coulomb Counting Method for State of Charge Estimation of Battery. In Proceedings of the 2024 IEEE 9th International Conference for Convergence in Technology (I2CT), Pune, India, 5–7 April 2024; pp. 1–3. [CrossRef]
36. Lee, J.; Won, J. Enhanced Coulomb Counting Method for SoC and SoH Estimation Based on Coulombic Efficiency. *IEEE Access* **2023**, *11*, 15449–15459. [CrossRef]
37. Wang, S.; Fan, Y.; Stroe, D.I.; Fernandez, C.; Yu, C.; Cao, W.; Chen, Z. Chapter 1–Lithium-ion battery characteristics and applications. In *Battery System Modeling*; Wang, S., Fan, Y., Stroe, D.I., Fernandez, C., Yu, C., Cao, W., Chen, Z., Eds.; Elsevier: Amsterdam, The Netherlands, 2021; pp. 1–46. [CrossRef]
38. Schürholz, D.; Schweighofer, B.; Neumayer, M.; Wegleiter, H. Investigation of the Coulombic Efficiency and the Superior Differential Capacity Degradation Analysis. *IEEE Sens. Lett.* **2023**, *7*, 1–4. [CrossRef]
39. Maithani, H.; Goel, S.K.; Uniyal, I.; Dubey, V.P.; Salyani, E. Advanced State Estimation Methods for Lithium-Ion Battery Cell- A Comprehensive Review. In Proceedings of the 2024 1st International Conference on Innovative Sustainable Technologies for Energy, Mechatronics, and Smart Systems (ISTEMS), Dehradun, India, 26–27 April 2024; pp. 1–6. [CrossRef]
40. Gismero, A.; Schaltz, E.; Stroe, D.I. Recursive State of Charge and State of Health Estimation Method for Lithium-Ion Batteries Based on Coulomb Counting and Open Circuit Voltage. *Energies* **2020**, *13*, 1811. [CrossRef]
41. Sun, X.; Chen, Q.; Zheng, L.; Yang, J. Joint Estimation of State-of-Health and State-of-Charge for Lithium-Ion Battery Based on Electrochemical Model Optimized by Neural Network. *IEEE J. Emerg. Sel. Top. Ind. Electron.* **2023**, *4*, 168–177. [CrossRef]
42. How, D.N.T.; Hannan, M.A.; Hossain Lipu, M.S.; Ker, P.J. State of Charge Estimation for Lithium-Ion Batteries Using Model-Based and Data-Driven Methods: A Review. *IEEE Access* **2019**, *7*, 136116–136136. [CrossRef]
43. Jongerden, M.; Haverkort, B. Which Battery Model to Use? *Softw. IET* **2010**, *3*, 445–457. [CrossRef]
44. Smith, K.A.; Rahn, C.D.; Wang, C.Y. Control oriented 1D electrochemical model of lithium ion battery. *Energy Convers. Manag.* **2007**, *48*, 2565–2578. [CrossRef]
45. Lin, C.; Tang, A.; Xing, J. Evaluation of electrochemical models based battery state-of-charge estimation approaches for electric vehicles. *Appl. Energy* **2017**, *207*, 394–404. [CrossRef]
46. Bartlett, A.; Marcicki, J.; Onori, S.; Rizzoni, G.; Yang, X.G.; Miller, T. Electrochemical Model-Based State of Charge and Capacity Estimation for a Composite Electrode Lithium-Ion Battery. *IEEE Trans. Control Syst. Technol.* **2016**, *24*, 384–399. [CrossRef]
47. Doyle, M.; Fuller, T.F.; Newman, J. Modeling of Galvanostatic Charge and Discharge of the Lithium/Polymer/Insertion Cell. *J. Electrochem. Soc.* **1993**, *140*, 1526. [CrossRef]
48. Chen, Y.; Huo, W.; Lin, M.; Zhao, L. Simulation of electrochemical behavior in Lithium ion battery during discharge process. *PLoS ONE* **2018**, *13*, e0189757. [CrossRef]
49. Fuller, T.F.; Doyle, M.; Newman, J. Simulation and Optimization of the Dual Lithium Ion Insertion Cell. *J. Electrochem. Soc.* **1994**, *141*, 1. [CrossRef]
50. Reddy, T. *Linden's Handbook of Batteries*, 4th ed.; McGraw Hill LLC.: New York, NY, USA, 2010.
51. Thiagarajan, R.S.; Subramaniam, A.; Kolluri, S.; Garrick, T.R.; Preger, Y.; Angelis, V.D.; Hyung Lim, J.; Subramanian, V.R. Efficient Reformulation of Linear and Nonlinear Solid-Phase Diffusion in Lithium-ion Battery Models using Symmetric Polynomials: Mass Conservation and Computational Efficiency. *J. Electrochem. Soc.* **2023**, *170*, 010528. [CrossRef]

52. Han, X.; Ouyang, M.; Lu, L.; Li, J. Simplification of physics-based electrochemical model for lithium ion battery on electric vehicle. Part II: Pseudo-two-dimensional model simplification and state of charge estimation. *J. Power Sources* **2015**, *278*, 814–825. [CrossRef]
53. Newman, J.; Tiedemann, W. Porous-electrode theory with battery applications. *AIChE J.* **1975**, *21*, 25–41. [CrossRef]
54. Fotouhi, A.; Auger, D.J.; Propp, K.; Longo, S.; Wild, M. A review on electric vehicle battery modelling: From Lithium-ion toward Lithium–Sulphur. *Renew. Sustain. Energy Rev.* **2016**, *56*, 1008–1021. [CrossRef]
55. Smith, K.; Wang, C.Y. Solid-state diffusion limitations on pulse operation of a lithium ion cell for hybrid electric vehicles. *J. Power Sources* **2006**, *161*, 628–639. [CrossRef]
56. Doyle, M.; Newman, J. The use of mathematical modeling in the design of lithium/polymer battery systems. *Electrochim. Acta* **1995**, *40*, 2191–2196. [CrossRef]
57. Ye, L.; Feng, Z. 14—Polymer electrolytes as solid solvents and their applications. In *Polymer Electrolytes*; Sequeira, C., Santos, D., Eds.; Woodhead Publishing Series in Electronic and Optical Materials; Woodhead Publishing: Cambridge, UK, 2010; pp. 550–582. [CrossRef]
58. Fan, C.; Higgins, M.D.; Widanage, W.D. Real-Time State of Charge Estimation of Electrochemical Model for Lithium-Ion Battery. In Proceedings of the 2019 IEEE Vehicle Power and Propulsion Conference (VPPC), Hanoi, Vietnam, 14–17 October 2019; pp. 1–6. [CrossRef]
59. Lotfi, N.; Landers, R.G.; Li, J.; Park, J. Reduced-Order Electrochemical Model-Based SOC Observer With Output Model Uncertainty Estimation. *IEEE Trans. Control Syst. Technol.* **2017**, *25*, 1217–1230. [CrossRef]
60. Cao, M.; Cao, Y.; Wang, C. Evaluation of Extended and Unscented Kalman Filter Algorithms for Battery State of Charge Estimation. In Proceedings of the 2023 42nd Chinese Control Conference (CCC), Tianjin, China, 24–26 July 2023; pp. 1291–1296. [CrossRef]
61. Fang, Y.Q.; Cheng, X.M.; Yin, Y.L. SOC Estimation of Lithium-Ion Battery Packs Based on Thevenin Model. In Proceedings of the Mechanical Engineering, Industrial Electronics and Informatization, Chongqing, China, 14–15 September 2013; Trans Tech Publications Ltd.: Stafa-Zurich, Switzerland, 2013; Volume 299, pp. 211–215. [CrossRef]
62. Chen, Y.; Huang, X.; Chen, Y. Lithium-Ion Battery State of Charge Estimation Based on a Second-order Central Difference Particle Filter Algorithm. In Proceedings of the 2024 IEEE 25th China Conference on System Simulation Technology and its Application (CCSSTA), Tianjin, China, 21–23 July 2024; pp. 538–542. [CrossRef]
63. Guo, R.; Shen, W. An Information Analysis Based Online Parameter Identification Method for Lithium-ion Batteries in Electric Vehicles. *IEEE Trans. Ind. Electron.* **2024**, *71*, 7095–7105. [CrossRef]
64. Ran, L.; Junfeng, W.; Haiying, W.; Gechen, L. Prediction of state of charge of Lithium-ion rechargeable battery with electrochemical impedance spectroscopy theory. In Proceedings of the 2010 5th IEEE Conference on Industrial Electronics and Applications, Taichung, Taiwan, 15–17 June 2010; pp. 684–688. [CrossRef]
65. Tari, L.; Bourelly, C.; Vitelli, M.; Milano, F.; Molinara, M.; Ferrigno, L. A Statistical Approach for Electrochemical Impedance Spectroscopy Analysis on LFP Batteries' State of Charge. In Proceedings of the 2023 IEEE International Workshop on Metrology for Industry 4.0 and IoT, Brescia, Italy, 6–8 June 2023; pp. 421–426. [CrossRef]
66. Uddin, M.S.; Kuh, A.; Weng, Y.; Ilić, M. Online bad data detection using kernel density estimation. In Proceedings of the 2015 IEEE Power and Energy Society General Meeting, Denver, CO, USA, 26–30 July 2015; pp. 1–5. [CrossRef]
67. Stighezza, M.; Ferrero, R.; Bianchi, V.; De Munari, I. Machine learning and impedance spectroscopy for battery state of charge evaluation. In Proceedings of the 2023 IEEE International Workshop on Metrology for Automotive (MetroAutomotive), Modena, Italy, 28–30 June 2023; pp. 24–29. [CrossRef]
68. Tian, J.; Xiong, R.; Shen, W.; Wang, J. A comparative study of fractional order models on state of charge estimation for lithium ion batteries. *Chin. J. Mech. Eng.* **2020**, *33*, 51 [CrossRef]
69. Bihn, S.; Rinner, J.; Witzenhausen, H.; Krause, F.; Ringbeck, F.; Sauer, D.U. Physics-Based Equivalent Circuit Model Motivated by the Doyle–Fuller–Newman Model. *Batteries* **2024**, *10*, 314. [CrossRef]
70. Sebastian, S.; Dong, B.; Zerrin, T.; Pena, P.; Akhavi, A.; Li, Y.; Ozkan, C.; Ozkan, M. Adaptive Fast Charging Methodology for Commercial Li-ion Batteries based on the Internal Resistance Spectrum. *Energy Storage* **2020**, *2*, e141. [CrossRef]
71. Howey, D.A.; Yufit, V.; Mitcheson, P.D.; Offer, G.J.; Brandon, N.P. Impedance measurement for advanced battery management systems. In Proceedings of the 2013 World Electric Vehicle Symposium and Exhibition (EVS27), Barcelona, Spain, 17–20 November 2013; pp. 1–7. [CrossRef]
72. Guo, R.; Hu, C.; Shen, W. An Adaptive Approach for Battery State of Charge and State of Power Co-Estimation With a Fractional-Order Multi-Model System Considering Temperatures. *IEEE Trans. Intell. Transp. Syst.* **2023**, *24*, 15131–15145. [CrossRef]
73. Guo, R.; Shen, W. Lithium-Ion Battery State of Charge and State of Power Estimation Based on a Partial-Adaptive Fractional-Order Model in Electric Vehicles. *IEEE Trans. Ind. Electron.* **2023**, *70*, 10123–10133. [CrossRef]

74. Din, E.; Schaef, C.; Moffat, K.; Stauth, J.T. A Scalable Active Battery Management System With Embedded Real-Time Electrochemical Impedance Spectroscopy. *IEEE Trans. Power Electron.* **2017**, *32*, 5688–5698. [CrossRef]
75. Beiranvand, H.; Placzek, J.M.; Liserre, M.; Zampardi, G.; Brogioli, D.C.; La Mantia, F. Review of Power Converter Topologies for Electrochemical Impedance Spectroscopy of Lithium-Ion Batteries. In Proceedings of the 2022 24th European Conference on Power Electronics and Applications (EPE'22 ECCE Europe), Hanover, Germany, 5–9 September 2022; pp. 1–10.
76. Wang, X.; Wei, X.; Dai, H.; Wu, Q. State Estimation of Lithium Ion Battery Based on Electrochemical Impedance Spectroscopy with On-Board Impedance Measurement System. In Proceedings of the 2015 IEEE Vehicle Power and Propulsion Conference (VPPC), Montreal, QC, Canada, 19–22 October 2015; pp. 1–5. [CrossRef]
77. Rezvanizaniani, S.M.; Liu, Z.; Chen, Y.; Lee, J. Review and recent advances in battery health monitoring and prognostics technologies for electric vehicle (EV) safety and mobility. *J. Power Sources* **2014**, *256*, 110–124. [CrossRef]
78. Ross, T. *Fuzzy Logic with Engineering Applications*, 3rd ed.; Wiley India Pvt. Limited: Hoboken, NJ, USA, 2011.
79. Singh, P.; Fennie, C.; Reisner, D. Fuzzy logic modelling of state-of-charge and available capacity of nickel/metal hydride batteries. *J. Power Sources* **2004**, *136*, 322–333. [CrossRef]
80. Shen, W.; Chan, C.; Lo, E.; Chau, K. Adaptive neuro-fuzzy modeling of battery residual capacity for electric vehicles. *IEEE Trans. Ind. Electron.* **2002**, *49*, 677–684. [CrossRef]
81. Saji, D.; Babu, P.S.; Ilango, K. SoC Estimation of Lithium Ion Battery Using Combined Coulomb Counting and Fuzzy Logic Method. In Proceedings of the 2019 4th International Conference on Recent Trends on Electronics, Information, Communication and Technology (RTEICT), Bangalore, India, 17–18 May 2019; pp. 948–952. [CrossRef]
82. G, S.; N, A.P.; Vaithilingam, C.A.; Phang, S.K.; Happonen, A. Extended Kalman-Bucy Filter with Fuzzy Hybrid Model for State of Charge Estimation of Lithium-Ion Batteries. In Proceedings of the 2023 Innovations in Power and Advanced Computing Technologies (i-PACT), Kuala Lumpur, Malaysia, 8–10 December 2023; pp. 1–6. [CrossRef]
83. Anwar, M.; Ashidqi, M.D.; Kaleg, S.; Adriyanto, F.; Cahyono, S.I.; Hapid, A.; Diharjo, K. State of Charge Monitoring System of Electric Vehicle Using Fuzzy Logic. In Proceedings of the 2018 International Conference on Sustainable Energy Engineering and Application (ICSEEA), Tangerang, Indonesia, 1–2 November 2018; pp. 34–38. [CrossRef]
84. Aggarwal, C.C. *Neural Networks and Deep Learning*; Springer: Berlin/Heidelberg, Germany, 2018; p. 497. [CrossRef]
85. Vidal, C.; Malysz, P.; Kollmeyer, P.; Emadi, A. Machine Learning Applied to Electrified Vehicle Battery State of Charge and State of Health Estimation: State-of-the-Art. *IEEE Access* **2020**, *8*, 52796–52814. [CrossRef]
86. Yang, F.; Zhang, S.; Li, W.; Miao, Q. State-of-charge estimation of lithium-ion batteries using LSTM and UKF. *Energy* **2020**, *201*, 117664. [CrossRef]
87. Yang, F.; Li, W.; Li, C.; Miao, Q. State-of-charge estimation of lithium-ion batteries based on gated recurrent neural network. *Energy* **2019**, *175*, 66–75. [CrossRef]
88. Apa, L.; Del Prete, Z.; Forconi, F.; Palermo, M.; Fulginei, F.R.; Rizzuto, E.; Sabino, L. Neural Network Approaches for State of Charge Prediction of Rechargeable Lithium Polymer Batteries. In Proceedings of the 2024 IEEE 22nd Mediterranean Electrotechnical Conference (MELECON), Porto, Portugal, 25–27 June 2024; pp. 236–241. [CrossRef]
89. Cardelli, E.; Crescimbini, F.; Fulginei, F.R.; Quercio, M.; Sabino, L. State-of-Charge assessment of Li-ion battery using Genetic Algorithm-Neural Network (GANN). In Proceedings of the 2024 International Conference on Artificial Intelligence, Computer, Data Sciences and Applications (ACDSA), Victoria, Seychelles, 1–2 February 2024; pp. 1–5. [CrossRef]
90. Yao, Q.; Kollmeyer, P.J.; Dah-Chuan Lu, D.; Emadi, A. A Comparison Study of Unidirectional and Bidirectional Recurrent Neural Network for Battery State of Charge Estimation. In Proceedings of the 2024 IEEE Transportation Electrification Conference and Expo (ITEC), Chicago, IL, USA, 19–21 June 2024; pp. 1–6. [CrossRef]
91. Chen, L.; Song, Y.; Lopes, A.M.; Bao, X.; Zhang, Z.; Lin, Y. Joint Estimation of State of Charge and State of Energy of Lithium-Ion Batteries Based on Optimized Bidirectional Gated Recurrent Neural Network. *IEEE Trans. Transp. Electrif.* **2024**, *10*, 1605–1616. [CrossRef]
92. Smola, A.; Scholkopf, B. A tutorial on support vector regression. *Stat. Comput.* **2004**, *14*, 199–222. [CrossRef]
93. Xu, Q.; Zhang, Y.; Li, C.; Wang, H.; Zhang, H.L.; Han, S. Battery Charge State Estimation Based on Support Vector Machine Hyperparameter Optimization. In Proceedings of the 2023 9th International Conference on Control Science and Systems Engineering (ICCSSE), Shenzhen, China, 16–18 June 2023; pp. 391–396. [CrossRef]
94. Hansen, T.; Wang, C.J. Support vector based battery state of charge estimator. *J. Power Sources* **2005**, *141*, 351–358. [CrossRef]
95. Yan, Q. SOC Prediction of Power Battery Based on SVM. In Proceedings of the 2020 Chinese Control And Decision Conference (CCDC), Hefei, China, 22–24 August 2020; pp. 2425–2429. [CrossRef]
96. Tang, A.; Huang, Y.; Liu, S.; Yu, Q.; Shen, W.; Xiong, R. A novel lithium-ion battery state of charge estimation method based on the fusion of neural network and equivalent circuit models. *Appl. Energy* **2023**, *348*, 121578. [CrossRef]
97. Wang, Q.; Ye, M.; Wei, M.; Lian, G.; Li, Y. Deep convolutional neural network based closed-loop SOC estimation for lithium-ion batteries in hierarchical scenarios. *Energy* **2023**, *263*, 125718. [CrossRef]

98. Yu, H.; Lu, H.; Zhang, Z.; Yang, L. A generic fusion framework integrating deep learning and Kalman filter for state of charge estimation of lithium-ion batteries: Analysis and comparison. *J. Power Sources* **2024**, *623*, 235493. [CrossRef]
99. Naguib, M.; Kollmeyer, P.; Emadi, A. Lithium-Ion Battery Pack Robust State of Charge Estimation, Cell Inconsistency, and Balancing: Review. *IEEE Access* **2021**, *9*, 50570–50582. [CrossRef]
100. Elvira, D.G.; Valderrama Blaví, H.; Bosque Moncusí, J.M.; Cid Pastor, A.; Garriga Castillo, J.A.; Martínez Salamero, L. Active Battery Balancing Via a Switched DC/DC Converter: Description and Performance Analysis. In Proceedings of the 2019 16th Conference on Electrical Machines, Drives and Power Systems (ELMA), Varna, Bulgaria, 6–8 June 2019; pp. 1–6. [CrossRef]
101. Chen, M.; Ma, G.; Liu, W.; Zeng, N.; Luo, X. An overview of data-driven battery health estimation technology for battery management system. *Neurocomputing* **2023**, *532*, 152–169. [CrossRef]
102. Xu, Y.; Ge, X.; Guo, R.; Shen, W. Recent advances in model-based fault diagnosis for lithium-ion batteries: A comprehensive review. *Renew. Sustain. Energy Rev.* **2025**, *207*, 114922. [CrossRef]